Model Chromia Surface Chemistry: C_2 Alkyl Fragment Reactions and Probe Molecule Interactions

John Daniel Brooks

Dissertation submitted to the faculty of Virginia Polytechnic Institute and State University in partial fulfillment of the requirements for the degree of

Doctor of Philosophy
In
Chemical Engineering

David F. Cox
S. Ted Oyama
Richey M. Davis
Brian E. Hanson
John R. Morris

September 29, 2010
Blacksburg, VA

Keywords: ethyl, ethylidene, ethylidyne, dehydrogenation, water, chromia

Model Chromia Surface Chemistry: C_2 Alkyl Fragment Reactions and Probe Molecule Interactions

John Daniel Brooks

ABSTRACT

The thermally induced reaction of chlorinated ethanes on the nearly-stoichiometric α-Cr_2O_3 ($10\bar{1}2$) surface results in the formation of gas phase hydrocarbons including ethylene, ethane, acetylene, 2-butene, 2-butyne and dihydrogen, and deposition of surface chlorine adatoms. No surface carbon or combustion products are observed in any reactions indicating no thermally induced C-C bond cleavage occurs and surface lattice oxygen is not incorporated into surface intermediates. A combination of photoemission and Auger electron spectroscopies indicates the surface reactions of the chlorinated ethanes proceed via C-Cl bond cleavage to form surface chlorine adatoms and surface C_2-alkyl hydrocarbon fragments (i.e. ethyl, ethylidene and ethylidyne). Temperature programmed desorption studies indicate that both ethyl and ethylidene intermediates are selective towards ethylene. However, ethylidyne is more selective towards acetylene, but also produces ethylene in significant quantities. Chlorine adatom deposition leads to deactivation of surface Cr reaction centers by simple site blocking.

The interaction of water with the nearly-stoichiometric α-Cr_2O_3 (0001) and ($10\bar{1}2$) surfaces is *structure sensitive*. Water is sensitive to the difference in coordination number of Cr surface cations between the two surfaces, and on the α-Cr_2O_3 (0001) surface, water has also demonstrated sensitivity to the degree of surface Cr cation reduction (and/or reduced coordination). These observations allowed for the development of a surface treatment recipe for the nearly-stoichiometric (0001) surface.

Acknowledgments

I would not be here today were it not for the efforts and influences of many people and experiences along the way. Their many roles have shaped and molded who I am and my view of the world. I thank the matchmaker and the president; the ornithologist, the historian and the chemist; the coach and the scoutmaster; my friends and family; my father, my mother and my stepmother; and the many people in the great state of South Carolina that purchased lottery tickets between 2001 and 2005.

Most of all, I thank my wife, Suzanne Edwards Brooks. I would have given up on graduate school long ago were it not for her persistent support and encouragement through the hardest times. She maintained the balance in our lives between working hard to achieve our goals while also taking the time to enjoy the ride. We have made so many wonderful memories together already, but I know that our best times are still ahead of us. This is only the beginning. I love and cherish her with all my heart.

Table of Contents

List of Figures

List of Tables

Chapter 1

Introduction

1.1 Catalytic Dehydrogenation of Ethane

Catalytic routes for ethane dehydrogenation to ethylene are desired to increase selectivity compared to traditional steam cracking processes. Various issues with the catalytic dehydrogenation process have prevented commercial implementation including the following: the process is highly endothermic requiring high temperature to acquire significant alkene yields [1]; the dehydrogenation reaction is expected to have low selectivity to alkenes because all C-H bonds in the molecule are equivalent in energy and are therefore equally likely to react; and the high temperatures required to overcome the kinetic barrier to C-H bond activation thermodynamically favor cracking reactions leading to lighter alkanes and coke formation [2]. While the kinetics of ethane dehydrogenation are controlled by the initial C-H bond activation [3], we postulate that the selectivity is controlled by the chemistry of different reaction intermediates and the characteristics of the catalytic active site over which the reaction is performed.

Supported chromia catalysts are used industrially in the catalytic dehydrogenation of C_3 and C_4 alkanes [2], and a number of studies have examined the applicability of chromia catalysts to the dehydrogenation and oxidative dehydrogenation of ethane [4-8]. The catalytically active sites for dehydrogenation chemistry are most likely coordinatively unsaturated Cr^{3+} cations sites [2].
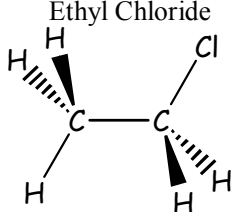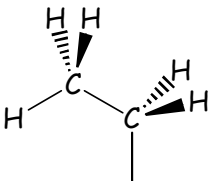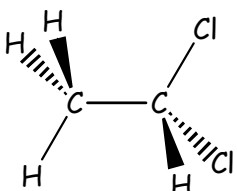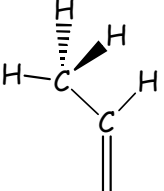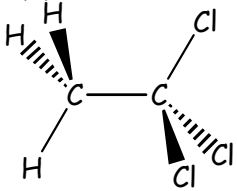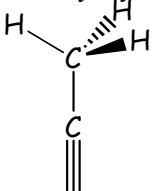
1.2 The purpose of this research project

In this ultra-high vacuum (UHV) surface science study, the reactions of C_2-alkyl fragments (ethyl, ethylidene and ethylidyne) are examined over a model, chromia, single crystal surface, α-Cr_2O_3 ($10\bar{1}2$). This is done in an effort to understand the relationship between selectivity of ethane dehydrogenation reactions and the specific intermediates formed from ethane by C-H bond scission. These C_2-alkyl fragments are of interest as the reaction intermediates expected from ethane by C-H bond cleavage from ethane on the same carbon.

1.3 Mimicking Catalytic Surface Reactions and C_2 Alkyl Fragment Formation

The homolytic and heterolytic C-H bond dissociation energies are 101 and 270 kcal/mol, respectively, to form an ethyl species from ethane [9,10]. However, the UHV conditions in this surface science study do not allow for the production of these intermediates directly from ethane via the initial C-H bond scission. Therefore, since carbon-halogen bonds are much weaker (C-Cl bonds ~85 kcal/mol [11]) than C-H bonds, the series of chlorinated ethanes shown in Table 1 are used to generate the C_2-alkyl fragments. The generation of surface bound hydrocarbon fragments by dissociative adsorption of halo-hydrocarbons has ample precedence in the surface science literature for metal surfaces [11-16]. In this study, the reactions of the chlorinated ethanes (Table 1) results in the creation of the desired surface fragments, as well as deposits of chlorine adatoms. In previous studies on the ($10\bar{1}2$) surface, site blocking by surface Cl adatoms deactivates the surface, and in some cases can change the kinetic barriers for surface reactions [17-21].

Table 1. Chlorinated ethane reactants used to obtain the three alkyl species.

Ethyl Chloride	Ethyl
1,1-Dichloroethane	Ethylidene
1,1,1-Trichloroethane	Ethylidyne

1.4 Probe Molecule Interactions: Water

The original research proposal set out to determine if the C_2-alkyl species reactions are *structure sensitive* by comparing the chemistry between two structurally unique surfaces, α-Cr_2O_3 $(10\bar{1}2)$ and (0001); however, characterization of the (0001) surface has proven non-trivial, inhibiting our complete understanding of preliminary studies of C_2-alkyl fragment chemistry. Therefore, in an effort to characterize the (0001) surface and the differences between the two surfaces, we have turned to studies of water adsorption as a probe of the surface properties. Water is the most widely studied molecule on well-defined, metal-oxide surfaces [22]. In this study, the interaction of water with the α-Cr_2O_3 $(10\bar{1}2)$ and (0001) surfaces provides insight into the difference in coordination number of surface Cr cations between the two surfaces; and on the (0001) surface provides a means by which to identify reduced Cr cations on sub-stoichiometric (0001) surfaces.

1.5 Model Chromia Surfaces Studied

Eskolaite, α-Cr_2O_3, is an insulator with the corundum structure and a band gap of 3.4 eV [23]. The bulk Cr^{3+} cations are six coordinate with nearest neighbor O^{2-} ligands in a distorted octahedral arrangement and one-third of the octahedral sites vacant [24]. The bulk O^{2-} anions are coordinated by chromium cations in a distorted tetrahedral fashion. The $(10\bar{1}2)$ and (0001) surfaces have the lowest energy of all the low-index surfaces [25], and are therefore, the most likely exposed faces in microcrystalline powders [26].

1.5.1 α-Cr_2O_3 $(10\bar{1}2)$

The α-Cr_2O_3 $(10\bar{1}2)$ single crystal surface has been characterized previously [27]. A ball model illustration of the ideal, stoichiometric surface is displayed in Figure 1. The
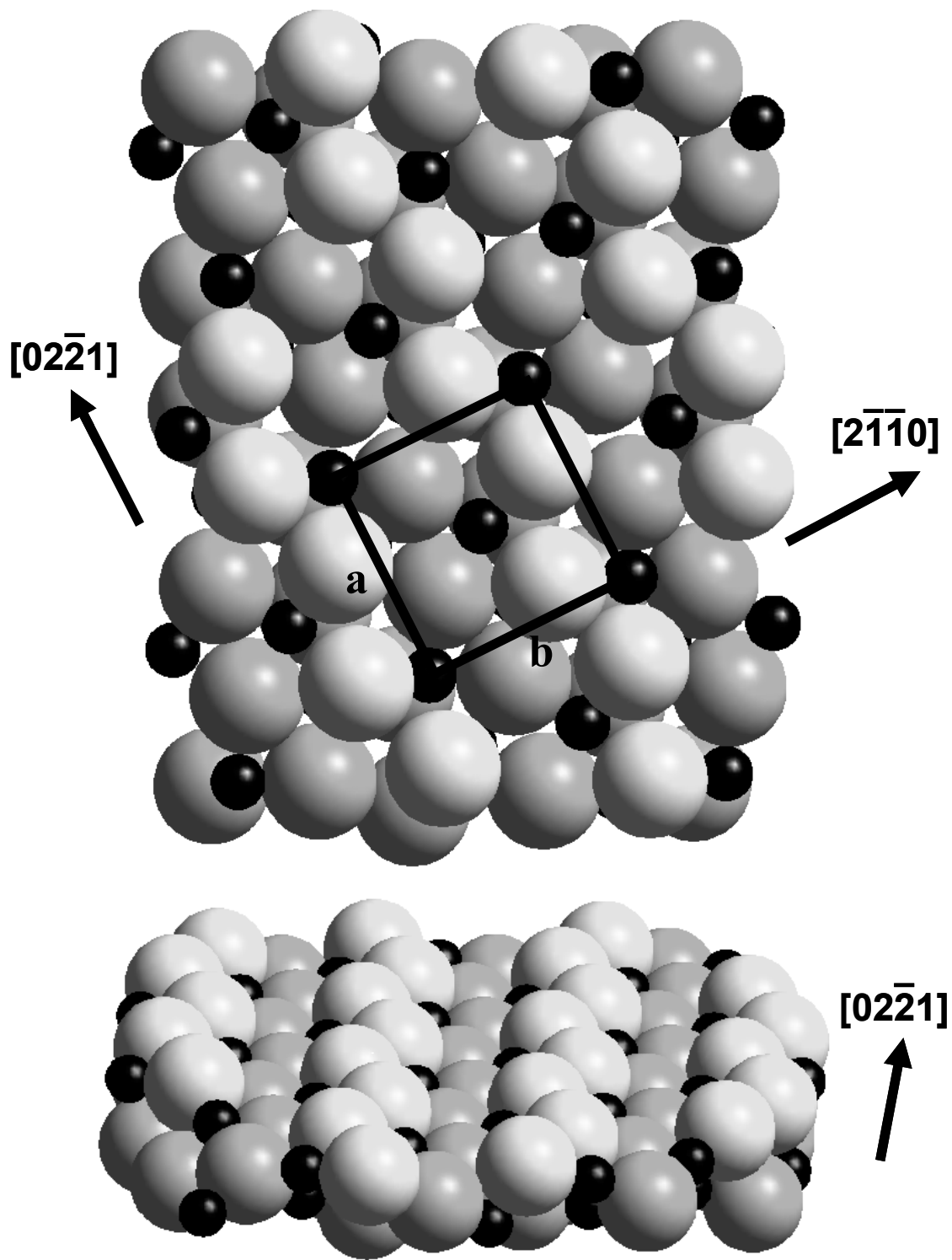
Figure 1. Ball model illustration of the ideal, nearly-stoichiometric α-Cr_2O_3 ($10\bar{1}2$) surface. The top view shows the surface periodicity (a:b = 0.94) looking down the $[10\bar{1}2]$ surface normal. The bottom view gives a perspective across the surface down $[02\bar{2}1]$ for a cross-section of one stoichiometric repeating layer. In both top and bottom views the small black spheres represent Cr^{3+} cations and the large gray spheres represent O^{2-} anions with increasing shading representing depth into the bulk.

($10\bar{1}2$) facet of α-Cr_2O_3 has the lowest energy of all low-index surfaces [25] and has a rectangular (almost square) periodicity, with a ratio of sides a/b = 0.94, as shown in Figure 1 [27]. Nearest neighbor Cr^{3+} cations on the ($10\bar{1}2$) surface are 3.65 Å apart. Energetic considerations dictate that the ($10\bar{1}2$) surface be terminated in a non-polar fashion, where one stoichiometric repeating unit includes the top five layers of atoms arranged as [O, Cr, O, Cr, O]. The O^{2-} anions comprising the top atomic layer are 3-coordinate with a pyramidal local coordination [28]. The Cr^{3+} cations in the second atomic layer are 5-coordinate, leaving one degree of coordinative unsaturation relative to their bulk counterparts [28]. The nearly-stoichiometric surface can be prepared by 2 keV Ar^+ ion bombardment and annealing to 900 K [27].

Oxygen exposure caps surface cations with terminal chromyl oxygen (Cr=O) [27]. The oxygen-terminated surface exposes 3-coordinate O^{2-} anions and terminal chromyl oxygen (Cr=O), leaving no coordination vacancies on the surface Cr cations [27]. In temperature programmed reaction studies of hydrocarbon fragments over α-Cr_2O_3 ($10\bar{1}2$), oxygenated gas phase products are only observed in the presence of terminal O species. Also, no combustion products (CO, CO_2 and H_2O) are produced on the nearly-stoichiometric surface [29], indicating that no lattice oxygen is incorporated into desorption products.

1.5.2 α-Cr_2O_3 (0001)

A ball model illustration representing the ideal, stoichiometric (0001) surface is shown in Figure 2. The surface has a hexagonal periodicity, and all chromium cations on the unrelaxed, bulk-terminated surface are an equal distance apart (4.96 Å). The surface
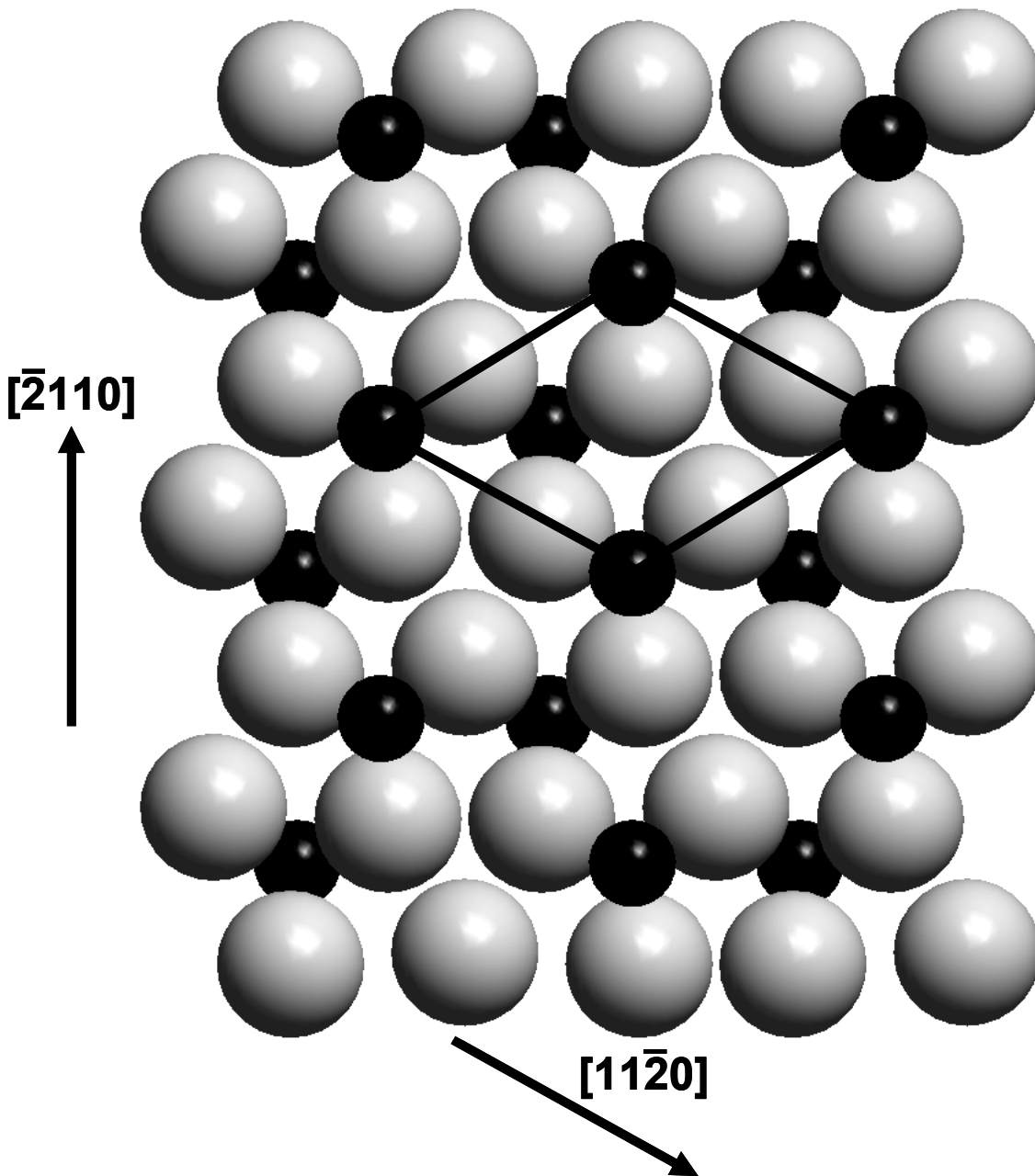
Figure 2. Ball model representation of the ideal, nearly-stoichiometric α-Cr$_2$O$_3$ (0001) surface assuming no relaxation. The black spheres represent the Cr^{3+} cations and the O^{2-} anions are represented by the larger gray spheres. This view is normal to the surface along the [0001] direction and shows the (1 x 1) hexagonal periodicity expected for a stoichiometric surface. The Cr-Cr interatomic distances are equivalently 4.961 Å apart for all Cr^{3+} cations in the same layer on the (0001) surface. Only the atomic layers are displayed, representing one stoichiometric repeating unit normal to the plane of the surface.

is non-polar, and one full stoichiometric repeating unit normal to the surface contains three atomic layers arranged as [Cr, 3O, Cr]. The topmost atomic layer is composed entirely of Cr cations. First-principles calculations suggest significant inward relaxation of the top-layer Cr^{3+} cations [30]. At the ideal (0001) surface, all Cr^{3+} cations are three coordinate with the same trigonal-pyramidal local coordination, and the O^{2-} anions in the second atomic layer are 3-coordinate. The Cr^{3+} surface cations have three degrees of coordinative unsaturation, while the O^{2-} surface anions have one relative to their bulk counterparts. All ions below the top two atomic layers are fully coordinated. Nearly-stoichiometric, thin-film surfaces have been reported following 500 eV Ar^+ ion bombardment and annealing to 850 K [31].

1.6 Experimental Methods

Experiments were conducted in two separate UHV systems, both with a base operating pressure of ~1 x 10^{-10} Torr. Temperature programmed desorption (TPD) and Auger electron spectroscopy (AES) experiments were conducted in an ion-pumped UHV chamber equipped with a Physical Electronics model 15-155 single-pass CMA for AES and an Inficon Quadrex 200 mass spectrometer for TPD. A broad-beam ion gun was used for sample cleaning.

The α-Cr_2O_3 crystals were oriented to within 1° of the ($10\bar{1}2$) and (0001) surfaces using Laue backreflection and polished to final mirror finish with 0.25 μm diamond paste. The sample was mechanically clamped onto a tantalum stage that was fastened to LN_2-cooled copper electrical conductors. A type K thermocouple was attached to the back of the single crystal through a hole in the stage using Aremco #569 ceramic cement. This arrangement allowed for direct measurement of the sample temperature.

AES data for the $(10\bar{1}2)$ and (0001) surface reaction studies were collected using a primary electron beam energy of 5 keV. Spectra were collected in N(E) mode and differentiated numerically. All AES measurements were collected at 800 K to avoid sample charging. Because of overlap between the primary oxygen and chromium AES peaks, the surface chromium concentration was followed by measuring the Cr $L_{2,3}M_{2,3}M_{2,3}$ (490 eV) peak-to-peak height. Atomic Cl/Cr ratios were estimated with AES using appropriate sensitivity factors for Cl LMM and Cr $L_{2,3}M_{2,3}M_{2,3}$ [27,32]. Electron stimulated reduction of the $(10\bar{1}2)$ surface (i.e. lattice oxygen removal) was not observed during AES experiments, consistent with other observations (see below and Ref. [27]) that the surface is quite nonreducible.

Soft X-ray photoelectron spectroscopy (XPS) was performed in a separate vacuum system at the U12a beamline at the National Synchrotron Light Source, Brookhaven National Laboratory. All photoemission spectra were collected at an instrumental resolution of 0.5 eV using 350 eV photons. Photoemission spectra are referenced to a Cr $2p_{3/2}$ binding energy of 576.9 eV [27,33].[1] Compensation for surface charging during synchrotron-based XPS was achieved with a Gammadata Scienta FG-300 flood gun using 0.5 eV electrons.

Aldrich 99.7% ethyl chloride (CH_3CH_2Cl), Spectrum 99.8% 1,1-dichloroethane (CH_3CHCl_2), Aldrich 99.8% 1,1,1-trichloroethane (CH_3CCl_3), Aldrich 99.5% vinyl chloride ($CH_2=CHCl$), Aldrich 99.99% ethane (CH_3CH_3), Specialty Gas Group 99.9% ethylene ($CH_2=CH_2$), Matheson 99% acetylene, Aldrich 99.9% dihydrogen (H_2), Aldrich 99% 2-butene (CH_3-CH=CH-CH_3), Aldrich 99% 2-butyne, Aldrich 99.9% water-d_2

---

[1] For XPS data taken at hν = 350 eV, the Cr 3p photoemission feature was used as an internal reference and compared to the Cr 2p3/2 feature in separate runs using hν = 650 eV.

(D$_2$O) and Matheson 99.997% oxygen (O$_2$) were used as received. Gas dosing was accomplished by backfilling the chamber through a variable leak valve. For TPD experiments, the sample surface was exposed to the dosed gas at 90 K and heated to above 800 K, using a linear temperature ramp of 2.5 K/s. The low heating rate was used to minimize the possibility of thermally fracturing the ceramic Cr$_2$O$_3$ sample. The mass spectrometer was equipped with a glass skimmer to minimize sampling desorption products from the crystal support hardware. All reported doses have been corrected for ion gauge sensitivity.[2]

A nearly-stoichiometric ($10\bar{1}2$) surface was prepared by 2 keV Ar$^+$ ion bombardment and annealing to 900 K [27]. A nearly-stoichiometric (0001) surface was prepared by initially oxidizing the clean surface by exposure to 1 x 10^{-7} Torr O$_2$ while heating from 300 to 900 K on a linear temperature ramp (1 K/s). The oxidation treatment induced K contamination on the surface, presumably by diffusion from the bulk to the surface. Therefore, following oxidation, the sample was bombarded with 500 eV Ar$^+$ ions and annealed to 900 K. Following this initial oxidation and mild-sputtering treatment the nearly-stoichiometric surface could be maintained for multiple preparations by 500 eV Ar$^+$ ion bombardment and annealing at 900 K. An ion bombarded and annealed (0001) surface was also prepared by 2 keV Ar$^+$ ion bombardment and annealing at 900 K.

---

[2] Ion gauge sensitivities of 4.0, 1.0 and 1.0 were used for ethyl chloride, water and oxygen, respectively [34]. Ion gauge sensitivitie of 1.39 and 2.3 were used for 1,1-dichloroethane and 1,1,1-trichloroethane, respectively. These ion gauge sensitivities were determined by using AES to estimate absolute Cl coverages from the reaction of low coverages of the respective chloro-hydrocarbon reactant where complete conversion to non-chlorinated products is observed in TPD. The estimate assumes a unity sticking coefficient for chloro-hydrocarbons at 90 K, and two Cl adatoms per reactant molecule.

Chapter 2

Reactions of ethyl groups on a model chromia surface: Ethyl Chloride on stoichiometric α-Cr$_2$O$_3$ (10$\bar{1}$2)

2.1 Introduction

The elementary reaction steps of ethyl species on metal surfaces have been examined because of their relevance to the catalytic dehydrogenation of ethane to ethylene [15,35-50]. Typically, the absorbed ethyl species are formed from the dissociative adsorption of halogenated molecules (ex., ethyl iodide, ethyl chloride, ethyl bromide) [15,35,38-47,50], while some groups have managed to form ethyl species by other methods such as UV-illumination [42] and coadsorption of di-σ-bonded CH$_2$=CH$_2$ and H atoms from a hot tungsten filament [49]. The ethyl species react via three primary pathways: β-hydride elimination to CH$_2$=CH$_2$, reductive elimination with hydrogen to CH$_3$CH$_3$ (α-addition) and reductive elimination with ethyl species to produce n-butane (C-C coupling).

2.2 Results

A combination of TPD and AES results reveals that CH$_3$CH$_2$Cl decomposes into ethylene (CH$_2$=CH$_{2(g)}$), ethane (CH$_3$CH$_{3(g)}$), dihydrogen (H$_{2(g)}$) and adsorbed chlorine. Gas phase products were identified by comparison of mass spectrometer fragmentation patterns to thermal desorption peak intensities. The relative intensities of four m/z signals were used to identify CH$_3$CH$_2$Cl (66, 64, 29, 27), CH$_2$=CH$_2$ (27, 26, 25, 24) and CH$_3$CH$_3$ (30, 29, 27, 26). Overlap of mass signals from ethyl chloride, ethane and ethylene was accounted for by subtracting overlapping contributions out of the raw mass spectrometer signal. Following these subtractions, the relative intensities of m/z

fragments for all hydrocarbon products formed were found to be in good agreement with mass spectrometer cracking patterns of hydrocarbon standards. Other products were excluded by a search that included m/z values ranging from 2 to 200. Specifically, no CO, CO_2, HCl, Cl_2, butane or any other oxygenated molecules, halogenated compounds or coupling products were produced from the reaction of ethyl chloride over the nearly-stoichiometric $(10\bar{1}2)$ surface. The desorption of H_2 rather than water and the lack of oxygenated products is an indication of the nonreducible nature of the surface. No surface carbon was detected following CH_3CH_2Cl decomposition; only chlorine was observed as a residual surface reaction product under the conditions of this study. All desorption traces and quantities have been corrected for mass spectrometer sensitivity.[3]

2.2.1. CH_3CH_2Cl thermal desorption

Desorption traces are shown in Figure 3 from the first in a series of consecutive 0.04 L doses and TPD runs of CH_3CH_2Cl started on the clean, nearly-stoichiometric α-Cr_2O_3 $(10\bar{1}2)$ surface. All desorbing species evolve between 300 and 600 K. The CH_3CH_2Cl reactant molecule desorbs at about 350 K while the products ethylene ($CH_2=CH_2$), ethane (CH_3CH_3), and H_2 desorb between 450 and 550 K. Comparison to desorption traces for the corresponding dosed molecule (not shown) indicate that the kinetics of the $CH_2=CH_2$, CH_3CH_3 and H_2 desorption are reaction-limited. (Desorption-limited evolution of ethylene and ethane occurs at 290 and 170 K, respectively [51], while the recombination of hydrogen atoms to H_2 occurs at 285 K [21].) $CH_2=CH_2$ desorption occurs at 500 K with a typical first-order peak shape. Note that the noisy section of the ethylene desorption trace between 300 and 400 K is an artifact of the

---

[3] Relative mass spectrometer sensitivity factors of 0.06 for ethyl chloride (m/z 64), 0.27 for ethylene (m/z 27), 0.15 for ethane (m/z 30), and 1.23 for H_2 (m/z 2) were determined experimentally.
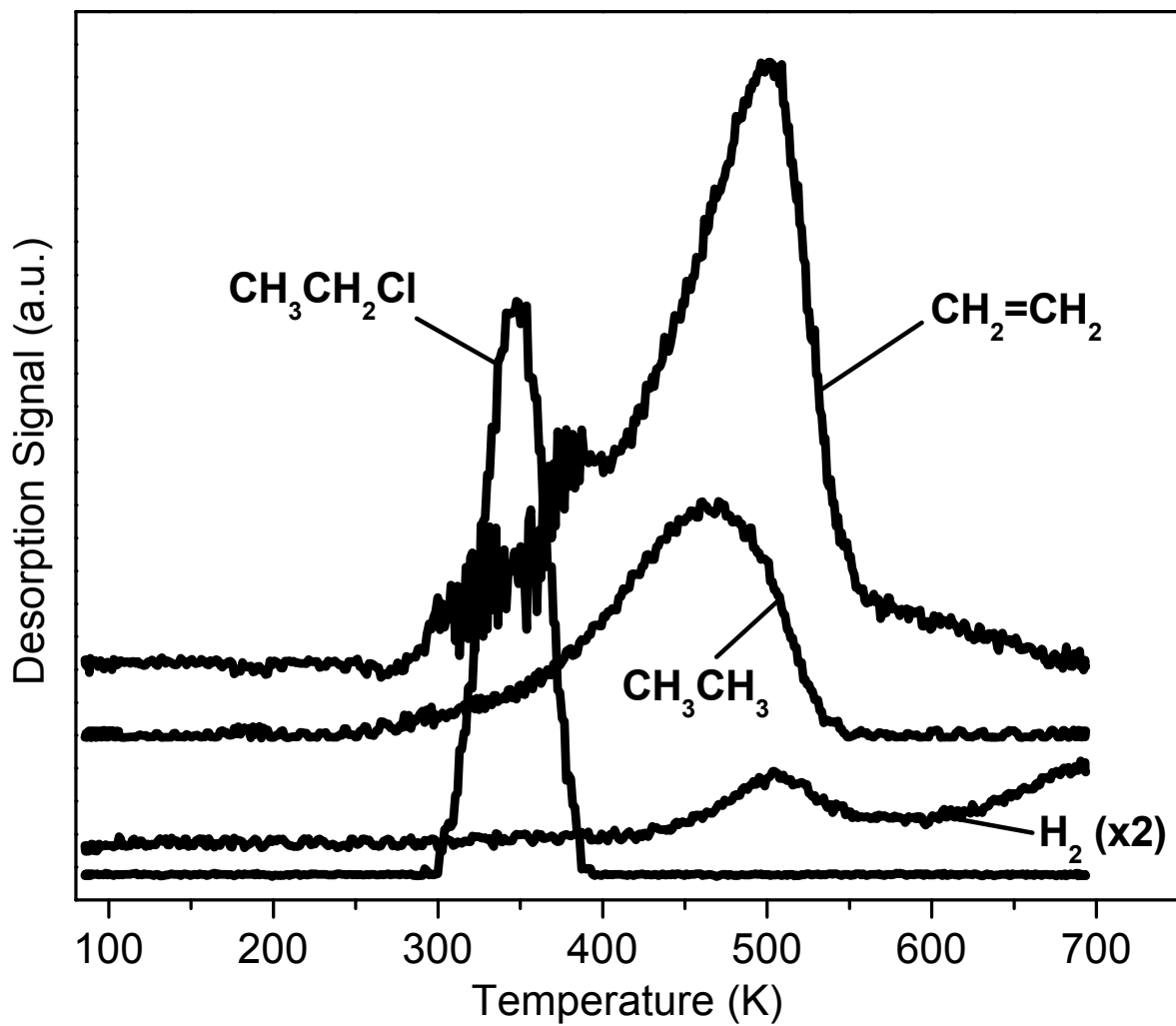
Figure 3. Thermal desorption following the first 0.04 L dose of CH_3CH_2Cl on the nearly-stoichiometric α-Cr_2O_3 ($10\bar{1}2$) surface

subtraction process used to remove the ethyl chloride contribution to the m/z 27 signal used to track ethylene. The apparent first-order activation energy of the surface reaction producing ethylene is 31 kcal/mol based on the Redhead analysis [52] and assuming a normal first-order pre-exponential factor of 10^{13} s^{-1}. The CH$_2$=CH$_2$ desorption is accompanied by both CH$_3$CH$_3$ (465 K) and H$_2$ (505 K) within the same temperature envelope, indicating that CH$_2$=CH$_2$, CH$_3$CH$_3$ and H$_2$ desorption products originate from a common surface intermediate with the same rate-limiting surface reaction step.

In addition to the data for small 0.04 L doses shown in Figure 3, we have examined the thermal desorption behavior over a significant range of ethyl chloride dose sizes, from 0.04 up to 2 L. For sequential TPD runs at varying Cl adatom coverage (data summarized in Figure 4), no variation in the ethylene desorption temperature is observed, indicating that the kinetics of the rate-limiting surface reaction are invariant with Cl coverage. For larger coverages given by ethyl chloride doses up to 2 L, no coupling products are observed, and no variation in the ethylene desorption temperature is observed, again indicating that the rate-limiting surface reaction is first-order and independent of coverage.

To determine the effect of Cl coverage on reactivity, a sequence of consecutive 0.04 L CH$_3$CH$_2$Cl doses and TPD runs were examined, and AES was used to follow the Cl coverage after each thermal desorption run. Figure 4 shows integrated areas of the desorption traces representing the amount of each desorbing species (corrected for mass spectrometer sensitivity[2]) on the left-hand axis, plotted with the respective Cl coverage measured following each thermal desorption run on the right-hand axis as a function of the total (cumulative) ethyl chloride exposure. After a cumulative exposure of 0.40 L

14
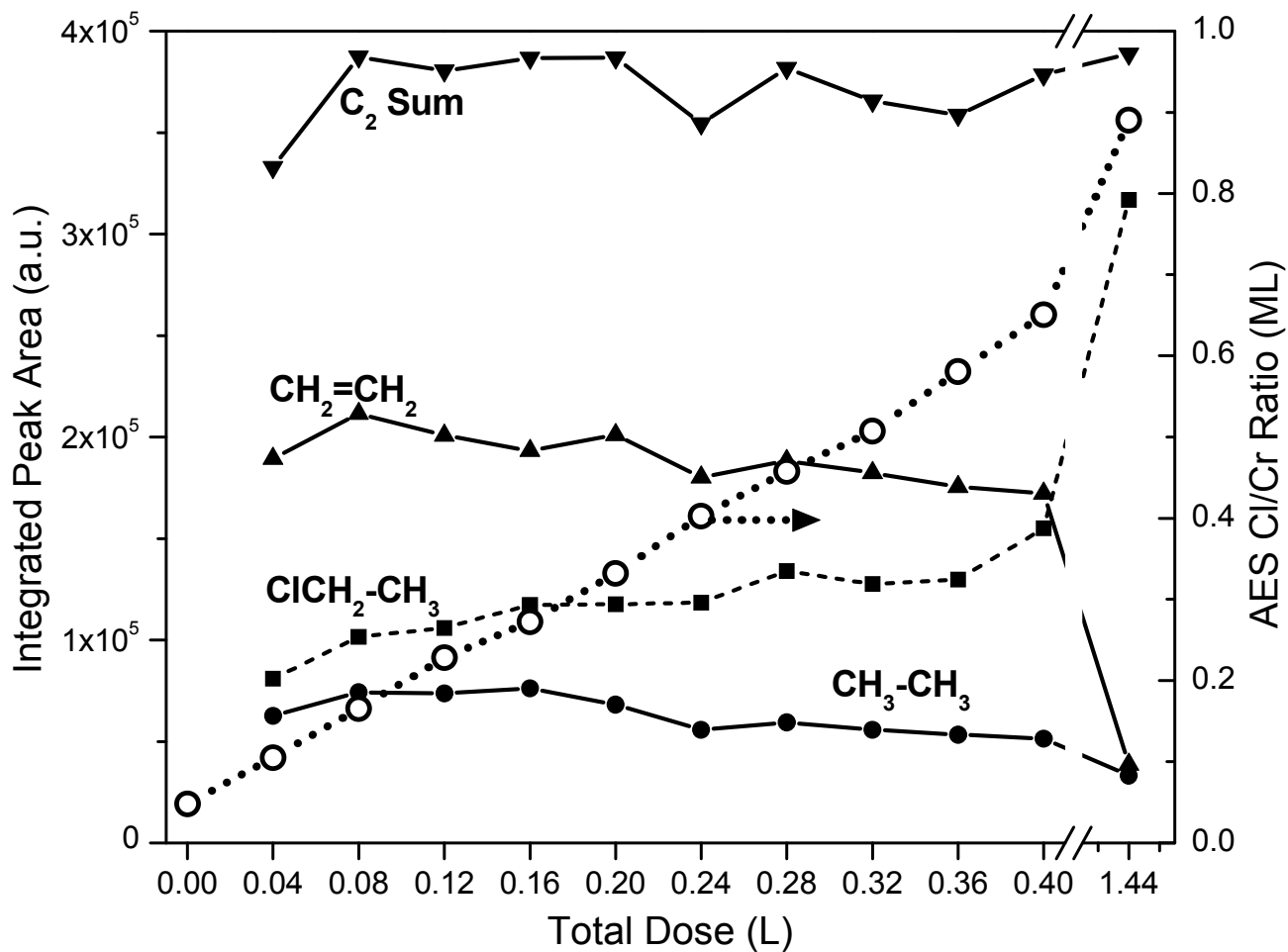
Figure 4. Variation in relative hydrocarbon desorption amounts for consecutive 0.04 L doses of CH_3CH_2Cl on the nearly-stoichiometric α-Cr_2O_3 ($10\bar{1}2$) surface. Corresponding Cl coverages are also displayed on the right-hand axis. Note the break in the scale along the x-axis. The break corresponds to two larger 0.5 L doses and thermal desorption runs used to drive up the coverage of surface Cl prior to the final 0.04 L dose.

of CH$_3$CH$_2$Cl, TPD runs were made with larger 0.5 L doses to drive up the Cl coverage. This process was followed by another 0.04 L dose and TPD run. This treatment is evident in the break in scale between 0.40 L and 1.44 L cumulative CH$_3$CH$_2$Cl dose in Figure 4.

For the initial 0.04 L doses, the Cl coverage increases linearly, indicating that a nearly constant amount of chlorine is deposited on the surface for each successive run. The amount of ethane and ethylene products varies slowly, with only a slight decrease in amounts up to 0.40 L cumulative exposure where Cl coverage is just less than 0.7 ML.[4] The amount of unreacted ethyl chloride shows the opposite trend, increasing slowly with each successive TPD run. Following the two larger (0.5 L) doses, the Cl coverage increases to 0.9 ML for a cumulative exposure of 1.44 L. At this higher Cl coverage, the amounts of product ethylene and ethane drop to near zero, and the amount of unreacted CH$_3$CH$_2$Cl reaches a maximum for the small 0.04 L dose size. The decreased surface reactivity for these higher CH$_3$CH$_2$Cl exposures and Cl coverages near 0.9 ML indicates that Cl adatoms block the active Cr^{3+} sites for the reaction as demonstrated previously [18,20,21,53].

Also shown in Figure 4 is the sum total of all desorbing C$_2$ species which includes the ethyl chloride reactant and ethylene and ethane products. The total amount of desorbing C$_2$ species is nominally constant, indicating that the ethyl chloride sticking coefficient for these small doses is independent of Cl coverage, although the reaction probability clearly decreases with increasing Cl coverage.

---

[4] 1 ML is defined as one adatom or molecule per surface Cr cation.

2.2.2. Post-reaction AES analysis

An AES spectrum for the clean surface is shown in Figure 5a, and displays the typical fingerprint of the nearly-stoichiometric α-Cr_2O_3 ($10\bar{1}2$) surface with Cr and O features in the range of 470-550 eV. A post-reaction AES spectrum (Figure 5b) taken after many sequential CH_3CH_2Cl exposures and TPD runs for an accumulated total dose of 1.44 L (same data shown in Figure 4) shows a chlorine feature near 181 eV characteristic of a Cl/Cr ratio of 0.29 corresponding to nearly monolayer coverage (i.e. AES Cl/Cr ratio of 0.32 [20]) of chlorine adatoms. No surface carbon (272 eV) is observed from the reaction of ethyl chloride in post-reaction AES measurements (Figure 5b). The surface O/Cr ratio measured before and after ethyl chloride TPD experiments show no change due to the deposition of surface chlorine. Therefore, no evidence is observed for the replacement of lattice oxygen by chlorine under these experimental conditions.

2.2.3. Soft X-ray photoelectron spectroscopy

Figure 6 shows the results of an XPS characterization of adsorbed ethyl chloride on the nearly-stoichiometric α-Cr_2O_3 ($10\bar{1}2$) surface. The sample was exposed to a 20 L dose of ethyl chloride at 120 K, heated briefly to 200 K to remove any multilayer contribution [54], then cooled to near 130 K and a photoemission spectrum collected. The sample was subsequently heated to consecutively higher temperatures. Following each heating treatment, the sample was cooled again to near 130 K and photoemission spectra were collected in an attempt to isolate the surface intermediate formed during the thermally-induced surface reaction of ethyl chloride.
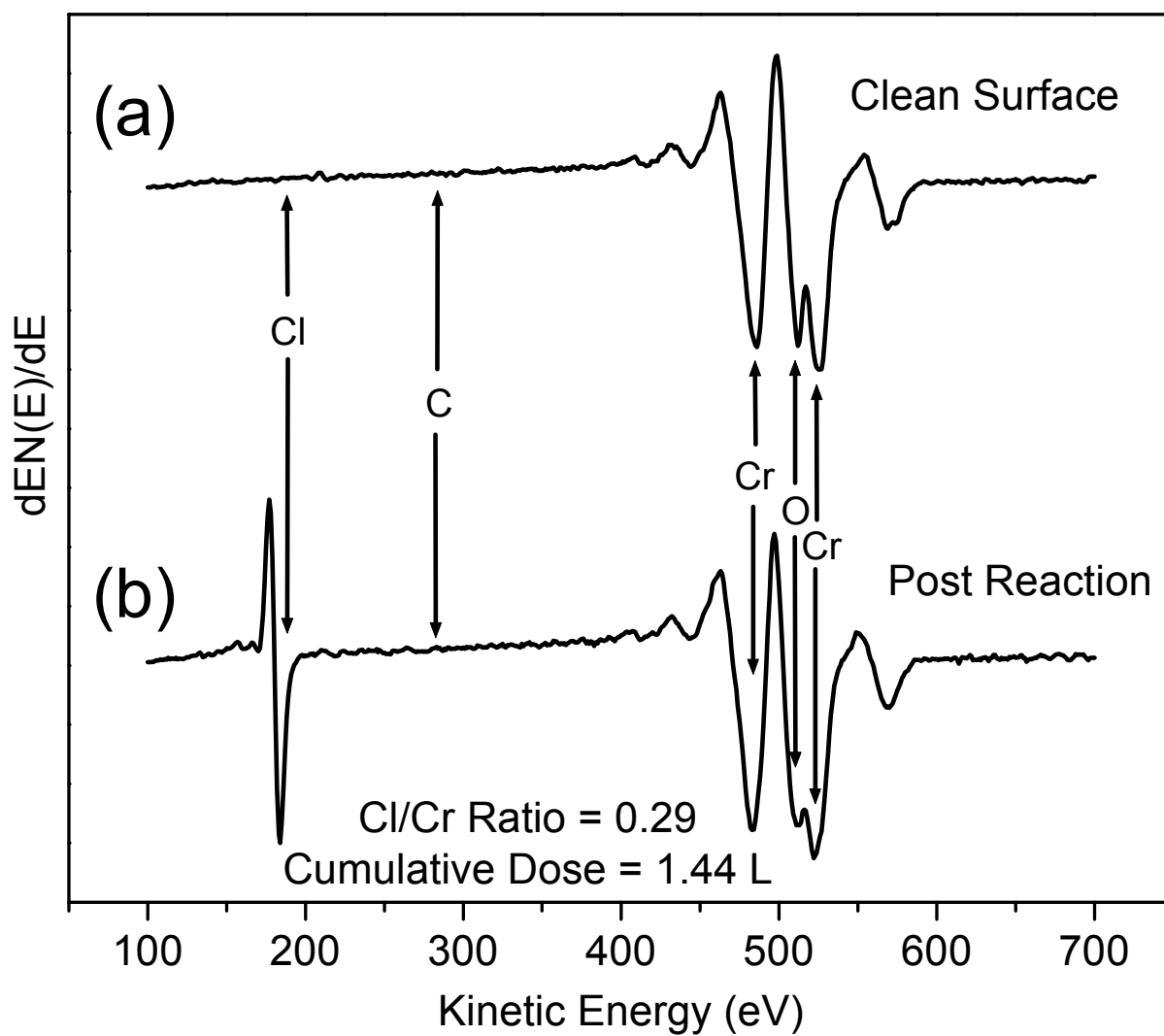
Figure 5. Auger electron spectra (AES) of both (a) clean, nearly-stoichiometric and (b) post-reaction Cl terminated α-Cr$_2$O$_3$ (10$\bar{1}$2) surfaces. Principle Auger electron peak locations are labeled and the Cl/Cr ratio of the post-reaction Cl terminated surface is indicated at the bottom of the plot.
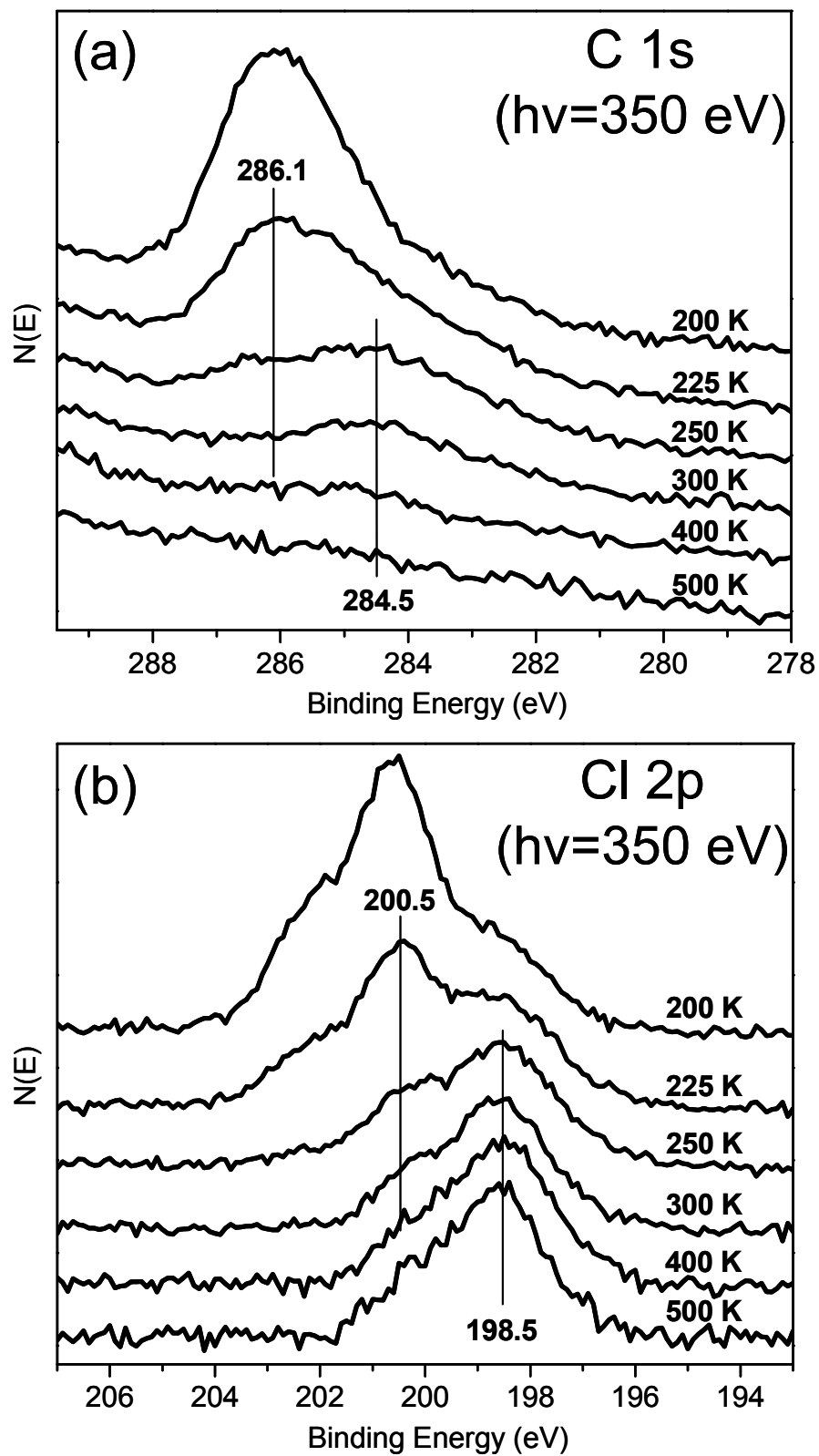
Figure 6. (a) C 1s and (b) Cl 2p XPS spectra. See text for details.

Figure 6a shows the series of XPS C 1s spectra, and Figure 6b shows the corresponding data for Cl 2p. The C 1s spectrum collected after dosing and heating to 200 K shows a broad, asymmetric, unresolved peak characteristic of multiple carbon features ranging from ~283 to 286 eV. For molecular ethyl chloride, two C 1s contributions are expected, one at higher binding energies (near 286 eV) attributable to the chlorinated carbon ($-CH_2Cl$), and a second at lower binding energies (near 284.5 eV) associated with the aliphatic methyl carbon (CH_3-) [33]. Two separate contributions near these binding energies are not resolved, but the maximum in the 200 K spectrum at 286.1 eV can be associated with the chlorinated carbon in ethyl chloride. As the temperature is increased, the intensity in the spectrum at 286.1 eV decreases, likely due to both molecular ethyl chloride desorption and C-Cl bond cleavage. After heating to 300 K, a peak centered at 284.5 eV is observed. This binding energy is consistent with alkyl carbon, and is attributed to the ethyl surface intermediate expected from the dissociation of ethyl chloride. Heating to temperatures up to 500 K results in a decrease and eventual loss of the C 1s feature over the temperature range associated with product desorption observing in TPD (Figure 3). The C 1s binding energy of 284.5 eV indicates that the ethyl intermediate is bound to surface Cr cations rather than O anions following C-Cl bond cleavage since C 1s binding energies for oxygenated carbons (ex., alkoxides, carboxylates, carbonates) typically fall at binding energies of 286 eV or greater [33,55]. Consistent with the AES results obtained under different exposure and reaction conditions, no residual carbon is observed in soft x-ray photoemission.

The Cl 2p spectra shown in Figure 6b exhibit a similar trend to the C 1s data. Multiple Cl species are observed following the dose, and high binding energy features are

lost as a result of heating. The Cl 2p spectrum collected after dosing and heating to 200 K shows three distinct contributions characteristic of a minimum of two sets of overlapping and poorly-resolved doublets with Cl $2p_{3/2}$ features at about 200.5 eV and 198.5 eV. Heating to temperatures up to 300 K results in a decrease and eventual loss of the high binding energy features and leaves a contribution primarily associated with a single unresolved Cl 2p doublet with a Cl $2p_{3/2}$ feature at 198.5 eV. Similar to the assignment for C 1s, the high binding energy features are attributed to Cl in molecular ethyl chloride, with the low binding energy features attributed to a Cl adatom surface reaction product. This low binding energy of the remaining Cl 2p doublet (Cl $2p_{3/2}$ at 198.5 eV) is characteristic of metal chloride [33], and is assigned to Cl adatoms bound at surface Cr sites. These XPS observations support earlier reports of the capping of surface Cr cations by halogen adatoms [18-21].

2.3 Discussion

The thermal decomposition of ethyl chloride to ethylene, ethane, dihydrogen and Cl adatoms occurs readily over the nearly-stoichiometric α-Cr_2O_3 $(10\bar{1}2)$ surface. From the XPS and AES results, it is clear that chlorine adatoms are deposited on the nearly-stoichiometric α-Cr_2O_3 $(10\bar{1}2)$ surface during TPD experiments. Since the weakest bond in alkyl chlorides is C-Cl with a bond energy of about 85 kcal/mol [56], it is reasonable to assume that the initial reaction step is the dissociation of adsorbed CH_3CH_2Cl via carbon-chlorine bond cleavage as seen previously on Ag [42,50]. Dissociation of CH_3CH_2Cl gives the expected surface ethyl intermediate, consistent with the C 1s binding energy observed in XPS following C-Cl bond cleavage.

The reaction-limited chemistry producing ethylene at 500 K along with ethane and dihydrogen is readily explained in terms of the decomposition of an ethyl reaction intermediate. β-hydride elimination is the most common decomposition pathway on metal surfaces for alkyl intermediates containing hydrogen atoms at the beta position [15,35,36,38-47,49], and directly forms ethylene, $CH_2=CH_2$. The liberated hydrogen atoms are then free to react with remaining surface ethyl fragments to form ethane, or may react with other surface hydrogen atoms to form dihydrogen. The proposed reaction mechanism may be represented by the following sequence of elementary steps:

$$CH_3CH_2Cl \rightarrow CH_3CH_2-_{(ads)} + Cl_{(ads)} \tag{2.1}$$

$$CH_3CH_2-_{(ads)} \rightarrow CH_2=CH_{2(g)} + H_{(ads)} \quad \text{(rate-limiting step)} \tag{2.2}$$

$$CH_3CH_2-_{(ads)} + H_{(ads)} \rightarrow CH_3CH_{3(g)} \tag{2.3}$$

$$H_{(ads)} + H_{(ads)} \rightarrow H_{2(g)} \tag{2.4}$$
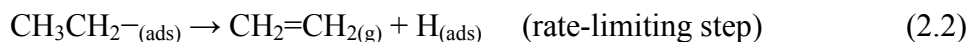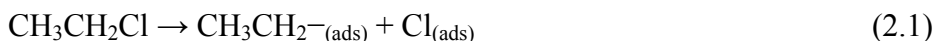
The CH_3CH_3 and H_2 products, reactions (2.3) and (2.4), are made possible by the presence of surface hydrogen released by the rate-limiting β-hydride elimination from ethyl intermediates; hence, the dehydrogenation step (2.2) is rate-limiting. It is noted that the temperature of the peak maximum for the subsequent products formed by hydrogen addition are slightly different than the 500 K observed for ethylene produced by ethyl dehydrogenation (ethane at 465 K and H_2 at 505 K) although both fall within the envelope of reaction temperatures where ethyl dehydrogenation to ethylene is observed. Reactions (2.3) and (2.4) compete for surface hydrogen, and since they are second-order elementary reactions the peak temperature can show dependence on surface coverage. In the lower temperature range where ethylene production is observed and the surface coverage of unreacted ethyl intermediates is highest, reaction (2.3) is the dominant

hydrogenation step. In the higher temperature range for ethylene production, the ethyl intermediate surface concentration is the lowest and H atom combination to H_2 (2.4) is the dominant hydrogenation step, where H_2 evolution temperature reasonably matches that for ethylene evolution.

The chlorine adatoms deposited on the nearly-stoichiometric α-Cr_2O_3 $(10\bar{1}2)$ surface during the reaction of ethyl chloride have no significant impact on the kinetics of the rate-limiting ethyl dehydrogenation step or the ethyl chloride sticking coefficient for small doses. They do, however, impact the reaction probability for ethyl chloride. For Cl coverages approaching 1 ML, the reaction probability for ethyl chloride decreases greatly (little product evolution is seen), and molecular CH_3CH_2Cl desorption becomes dominant. Hence, the decrease in reactivity is brought about by Cl deposition. The observed binding energy of Cl adatoms in XPS is consistent with a metal chloride, and indicates that Cl adatoms block active Cr^{3+} sites for reaction, consistent with earlier suggestions [20].

In the catalysis literature, deactivation of powdered Cr_2O_3 catalysts has been attributed to carbon deposition [57], and to the formation of inactive crystalline phases at the surface that isolate cations from the surface [58]. In this work, no carbon residue is deposited on the α-Cr_2O_3 $(10\bar{1}2)$ surface as a result of ethyl fragment decomposition and dehydrogenation under the conditions of our experiments. These results suggest that ethyl fragments are not a major intermediate in coke production, at least not on this simple chromia surface where the available cation and anion sites expose primarily a single coordination vacancy.

2.4 Conclusions

The reaction of ethyl species was investigated on the nearly-stoichiometric α-Cr_2O_3 $(10\bar{1}2)$ surface under UHV conditions via the dissociative adsorption of CH_3CH_2Cl. Reaction products include $CH_2=CH_2$, CH_3CH_3 and H_2. The rate-limiting surface reaction step is β-elimination from a surface ethyl intermediate. Chlorine adatoms from the decomposition reaction deactivated the surface by simple Cr^{3+} site blocking as the chlorine coverage approached one monolayer [20]. No surface carbon was observed in post-reaction AES and XPS, indicating that ethyl species are likely not primary coke forming intermediates on $(10\bar{1}2)$ facets of α-Cr_2O_3.

Chapter 3

Reactions of ethylidene groups on a model chromia surface: 1,1-Dichloroethane on stoichiometric α-Cr$_2$O$_3$ (10$\bar{1}$2)

3.1 Introduction

Supported chromia catalysts are used industrially in the catalytic dehydrogenation of C$_3$ and C$_4$ alkanes [2], and a number of studies have examined the applicability of chromia catalysts to the dehydrogenation and oxidative dehydrogenation of ethane [4-8]. Ethylidene species are of interest for this reaction system because they are a secondary C$_2$ reaction intermediate, after ethyl species, expected from ethane by cleavage of two C-H bonds on the same carbon. In this study, the reactions of ethylidene fragments are examined over a model single crystal chromia surface, α-Cr$_2$O$_3$ (10$\bar{1}$2). Surface ethylidene species are generated via the thermal dissociation of 1,1-dichloroethane.

The reaction of ethylidene species prepared by the dissociative adsorption of 1,1-dihaloethanes has been studied on a limited variety of metal surfaces [11-14,16]. On both Cu (100) [11] and Ag (111) [14], ethylidene moieties favor coupling to 2-butene. On Pt (111) [13], both α-hydrogen elimination to ethylidyne and a 2,1-hydrogen shift to ethylene are observed. A combination of theoretical [59] and experimental [60] evidence on Pd (111) suggests that ethylidene undergoes α-hydrogen abstraction to form ethylidyne species. Therefore, precedence exists in the surface science literature for the reaction of ethylidene species to couple to form 2-butene, dehydrogenate from the α carbon to form ethylidyne, and isomerize via a 2,1-hydrogen shift to ethylene.

25

3.2 Results

3.2.1. Reaction products

TPD, AES and XPS reveal that CH_3CHCl_2 reacts primarily to ethylene

($CH_2=CH_{2(g)}$) and chlorine adatoms on $\alpha-Cr_2O_3(10\bar{1}2)$; however, trace quantities of

ethane ($CH_3CH_{3(g)}$), acetylene, 2-butene ($CH_3CH=CHCH_{3(g)}$), and H_2 are also observed.

As will be described below, the selectivity of the reaction is dependent on the Cl adatom

coverage. As a result, the reaction was studied primarily using small gas exposures so

that variations in reactivity can be related to the extent of Cl deposition.

Gas phase products were identified in TPD by comparison of mass spectrometer

fragmentation patterns to thermal desorption peak intensities. The relative intensities of

four m/z signals were used to identify CH_3CHCl_2 (85, 83, 65, 63), $CH_2=CH_2$ (27, 26, 25,

24), CH_3CH_3 (30, 29, 28, 27), acetylene (26, 25, 24, 13) and 2-butene (41, 39, 56, 55).

Overlap of mass signals from 1,1-dichloroethane, ethylene, ethane, acetylene and 2-

butene was accounted for by subtracting overlapping contributions out of the raw mass

spectrometer signal. Following these subtractions, the relative intensities of m/z

fragments for all hydrocarbon products formed were found to be in good agreement with

mass spectrometer fragmentation patterns of hydrocarbon standards. Other products

were excluded by a search that included m/z values ranging from 2 to 200. Specifically,

no CO, CO_2, HCl, Cl_2, or any other oxygenated molecules, halogenated compounds or

coupling products were produced from the reaction of 1,1-dichloroethane over the nearly-

stoichiometric $(10\bar{1}2)$ surface. The lack of oxygenated products is an indication of the

nonreducible nature of the surface. No surface carbon was detected with AES following

the reaction of CH_3CHCl_2 in TPD; only chlorine was observed as a residual surface

reaction product. All desorption traces and quantities have been corrected for mass spectrometer sensitivity.[5]

3.2.1.1. Primary chemistry: ethylene production

Figure 7 shows TPD traces for ethylene, the primary reaction product, and the 1,1-dichloroethane reactant produced from a 0.27 L (1 L $\equiv$ 1×10^{-6} torr·sec) dose of 1,1-dichloroethane at 90 K on a *partially chlorinated* surface. The partially chlorinated surface was produced by four prior 0.27 L doses and TPD runs on an initially clean surface. As determined by AES (below), this treatment results in a Cl coverage of ~ 0.6 ML.[6] Because of the high molecular weight of dichloroethane (MW=99), a 0.27 L exposure to 1,1-dichloroethane corresponds to less than 8% of monolayer coverage.[7] All desorbing species evolve between 250 and 500 K. The CH_3CHCl_2 reactant molecule desorbs in two features near 310 and 410 K, while the CH_2=CH_2 product desorbs at 385 K. Also shown is a TPD trace for H_2. The lack of an H_2 desorption signal indicates that no H-elimination reactions take place under these reaction conditions. Previous work on this surface with ethyl [17] and vinyl [18] species demonstrates that H-elimination reactions are accompanied by H_2 desorption.

The production of CH_2=CH_2 at 385 K in Figure 7 is reaction-limited since dosed CH_2=CH_2 (not shown) desorbs at 290 K [51]. The reaction order is not obvious by qualitative inspection of the peak shape in Figure 7. However, a variety of coverages were examined using 1,1-dichloroethane doses ranging from 0.2 to 5 L (not shown), and

---

[5] Relative mass spectrometer sensitivity factors of 0.086 for 1,1-dichloroethane (m/z 63), 0.41 for ethylene (m/z 27), 0.13 for ethane (m/z 30), 4.3 for dihydrogen (m/z 2), 0.52 for 2-butene (m/z 41) and 0.67 for acetylene (m/z 26) were determined experimentally.
[6] 1 ML is defined as one adatom or molecule per surface Cr cation.
[7] Estimates of the 1,1-dichloroethane coverage are calculated assuming a unity sticking coefficient at 90 K and a total Cr surface site density of 7.5×10^{14} Cr/cm^2.
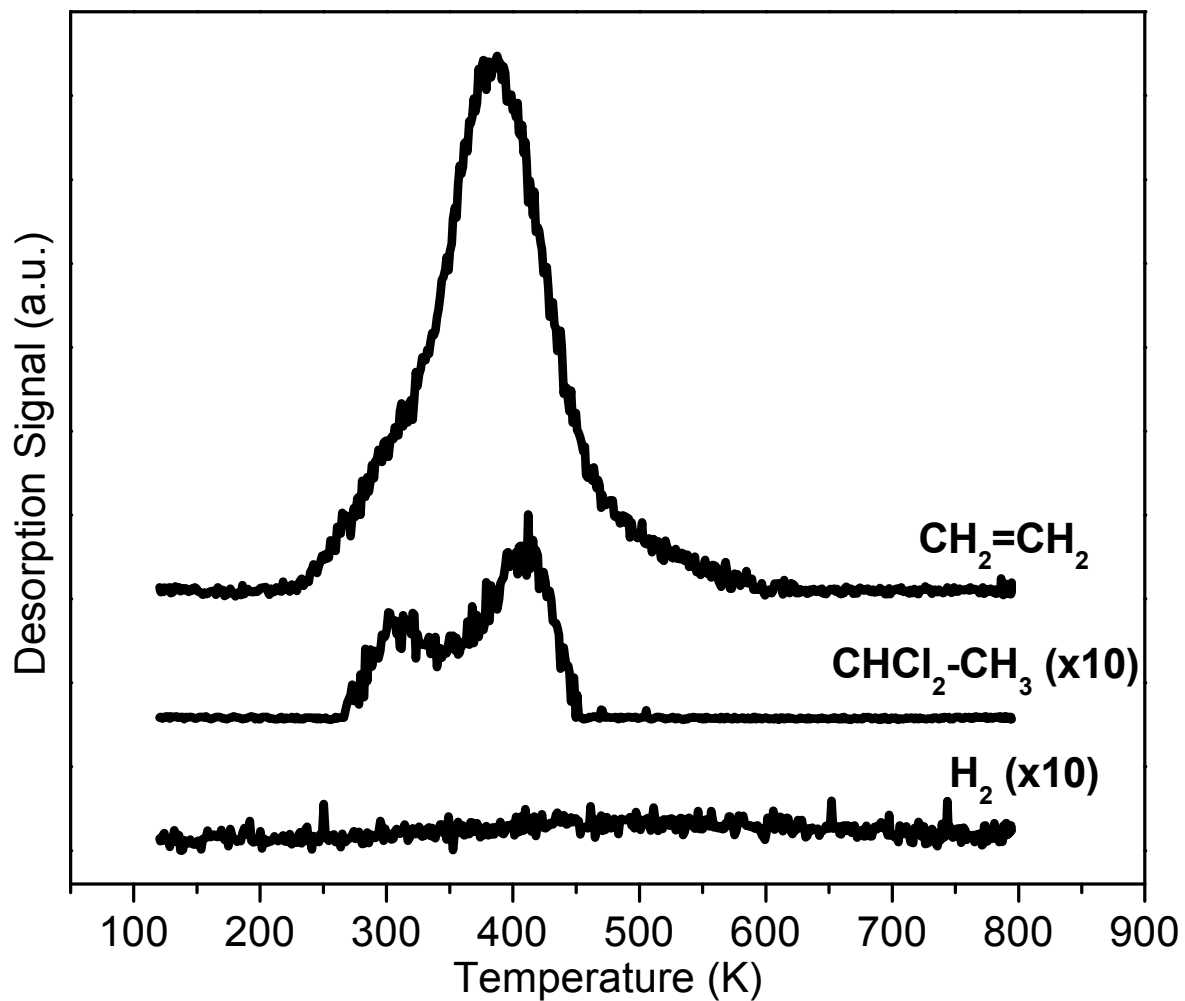
Figure 7. TPD following the fifth 0.27 L dose of CH_3CHCl_2 on the partially chlorinated α-Cr_2O_3 ($10\bar{1}2$) surface. The baselines have been offset for clarity.

the temperature maximum of the ethylene desorption signal remained essentially constant for widely varying amounts of ethylene produced. Therefore, the kinetics of the rate-limiting surface reaction step for ethylene production is thought to be first order [52]. The apparent first-order activation energy of the reaction producing $CH_2=CH_2$ at 385 K is 24 kcal/mol based on the Redhead analysis [52], assuming a normal, first-order, pre-exponential of 10^{13} s^{-1}.

The surface chemistry giving rise to $CH_2=CH_2$ is readily explained by the first-order, intramolecular isomerization of a surface ethylidene fragment ($CH_3CH=$) formed from the dissociative adsorption of CH_3CHCl_2. The isomerization is described as intramolecular because the rate-limiting step is first-order and no evidence for a separate H-elimination reaction (and subsequent H addition) is observed. In general terms, the chemistry can be described by the following two reactions: (3.1) dissociative adsorption of 1,1-dichloroethane to ethylidene and surface chlorine adatoms via C–Cl bond scission, and (3.2) the rate-limiting intramolecular isomerization of ethylidene to ethylene.

$$CH_3CHCl_2 \rightarrow CH_3CH=_{(ads)} + 2\ Cl_{(ads)} \qquad (3.1)$$

$$CH_3CH=_{(ads)} \rightarrow CH_2=CH_2 \qquad (3.2)$$
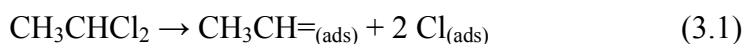
Figure 8 illustrates the variation in the amounts of desorbing species (reactant and products) due to changes in the surface Cl coverage. Consecutive 0.27 L doses and TPD runs were performed, starting with a clean, nearly-stoichiometric surface. AES was used to quantify the amount of deposited Cl after each TPD run. Integrated TPD peak areas of the desorption traces (corrected for mass spectrometer sensitivity[5]) representing the amount of each species are plotted on the left-hand axis, and the Cl coverage measured with AES following each TPD run is plotted on the right-hand axis, all as a function of
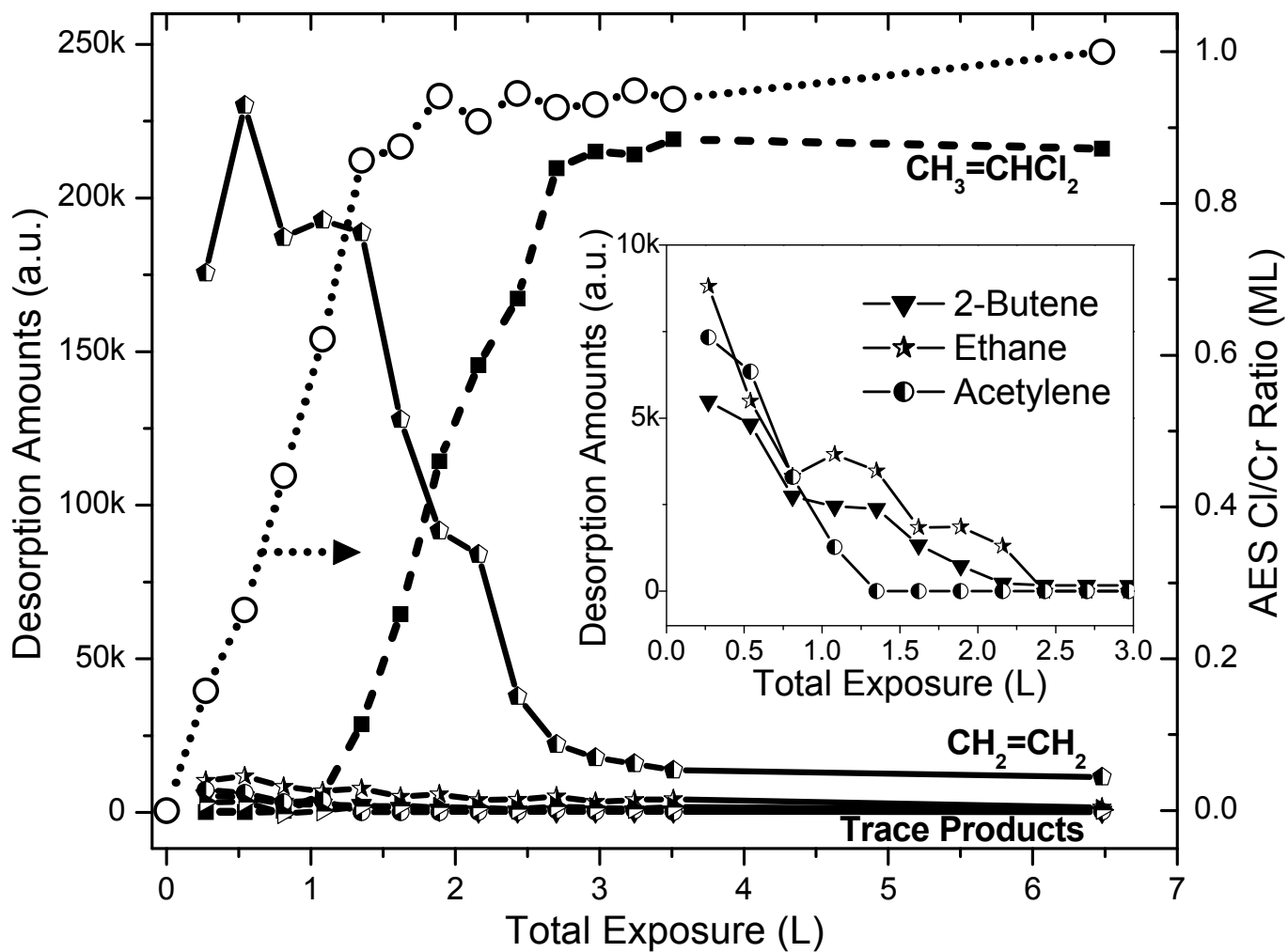
Figure 8. Variation in the relative hydrocarbon desorption amounts for consecutive 0.27 L doses of CH_3CHCl_2 on the nearly-stoichiometric α-Cr_2O_3 (10$\bar{1}$2) surface. Corresponding Cl/Cr ratios are also displayed on the right-hand axis scaled so that unity represents 1 Cl adatom per surface Cr cation. The inset shows the trace products for clarity.

the total (cumulative) CH_3CHCl_2 exposure. After a cumulative exposure of 3.5 L of CH_3CHCl_2, a TPD run was made with a larger 2.7 L dose in an attempt to saturate the surface with Cl adatoms. This process was followed by another 0.27 L dose and TPD run.

From Figure 8 it is seen that Cl coverage increases with successive TPD runs reaching a near monolayer coverage for the largest cumulative dose. For the first four doses, there is little or no desorption of the CH_3CHCl_2 reactant, and the maximum production of ethylene is observed. For the fifth and later doses, the amount of desorbing reactant increases nearly linearly before rolling over to an essentially constant value as the Cl coverage approaches ~0.9 ML. A drop off in the amount of the ethylene primary product accompanies the increase in the amount of the 1,1-dichloroethane reactant. The data indicate that that the reaction probability decreases for CH_3CHCl_2 with increasing Cl coverage on the surface. The decreased surface reactivity for total CH_3CHCl_2 exposures above ~ 2.5 L and Cl coverages near 0.9 ML indicates that Cl adatoms block the active Cr^{3+} sites for the reaction as demonstrated previously [17,18,20,21].

For the 1,1-dichloroethane reactant, the behavior of the two desorption features seen in Figure 7 vary differently with increasing Cl coverages and increasing amounts of the desorbing reactant (not shown). For total doses between 1 L and 2.5 L, the high temperature (410 K) feature increases in intensity at constant temperature and saturates, while the low temperature feature (310K) feature increases but shifts to lower temperatures (< 250 K). The trend towards lower temperatures of the 310 K feature indicates a decreased activation barrier to desorption for increasing coverage of the reactant molecule likely due to intermolecular repulsive forces within the adsorbed layer.

The persistence of the high temperature feature at 410 K suggests that some other first-order process is rate-limiting besides the simple desorption of an adsorbed CH_3CHCl_2 molecule (see section 3.3.2).

3.2.1.2. Trace chemistry: acetylene, ethane, dihydrogen and 2-butene production

The inset of Figure 8 shows the trace products: 2-butene, ethane and acetylene. Less than 5% of all CH_3CHCl_2 that reacts forms these trace products. The amounts of all trace products decreases rapidly as the total exposure to CH_3CHCl_2 increases, whereas the primary product ethylene remains more persistent. This rapid drop off in the amount of the trace products within the first few consecutive doses is consistent with selective poisoning of the reaction sites by deposited Cl adatoms. Due to the low selectivity and rapid decline coincident with Cl adatom deposition, the trace chemistry producing ethane and acetylene is likely due to a minority of reaction sites, possibly associated with surface defects (i.e. steps, kinks, point defects, etc.). An estimate of the site population producing the trace chemistry relative to the total Cr site population is less than 2.5% of the total.[8]

Figure 9 shows a typical set of TPD traces following the first 0.27 L dose of CH_3CHCl_2 at 90 K on a clean, nearly-stoichiometric α-Cr_2O_3 ($10\bar{1}2$) surface. The $CH_2=CH_2$ product from the clean surface has a high-temperature tail extending to 700 K that is not present on the partially chlorinated surface in Figure 7. 2-Butene production occurs primarily at 340 K, with a smaller contribution at 470 K. CH_3CH_3 production occurs at 430 K, acetylene evolves near 640 K, and H_2 desorbs in a range from about 400-750 K with a primary maximum at 665 K and a smaller, low temperature feature

---

[8] An estimate of the minority site population was calculated based on the total fraction of reacted dichloroethane producing ethane and acetylene assuming one reaction per site with the site poisoned by the deposited Cl adatom.
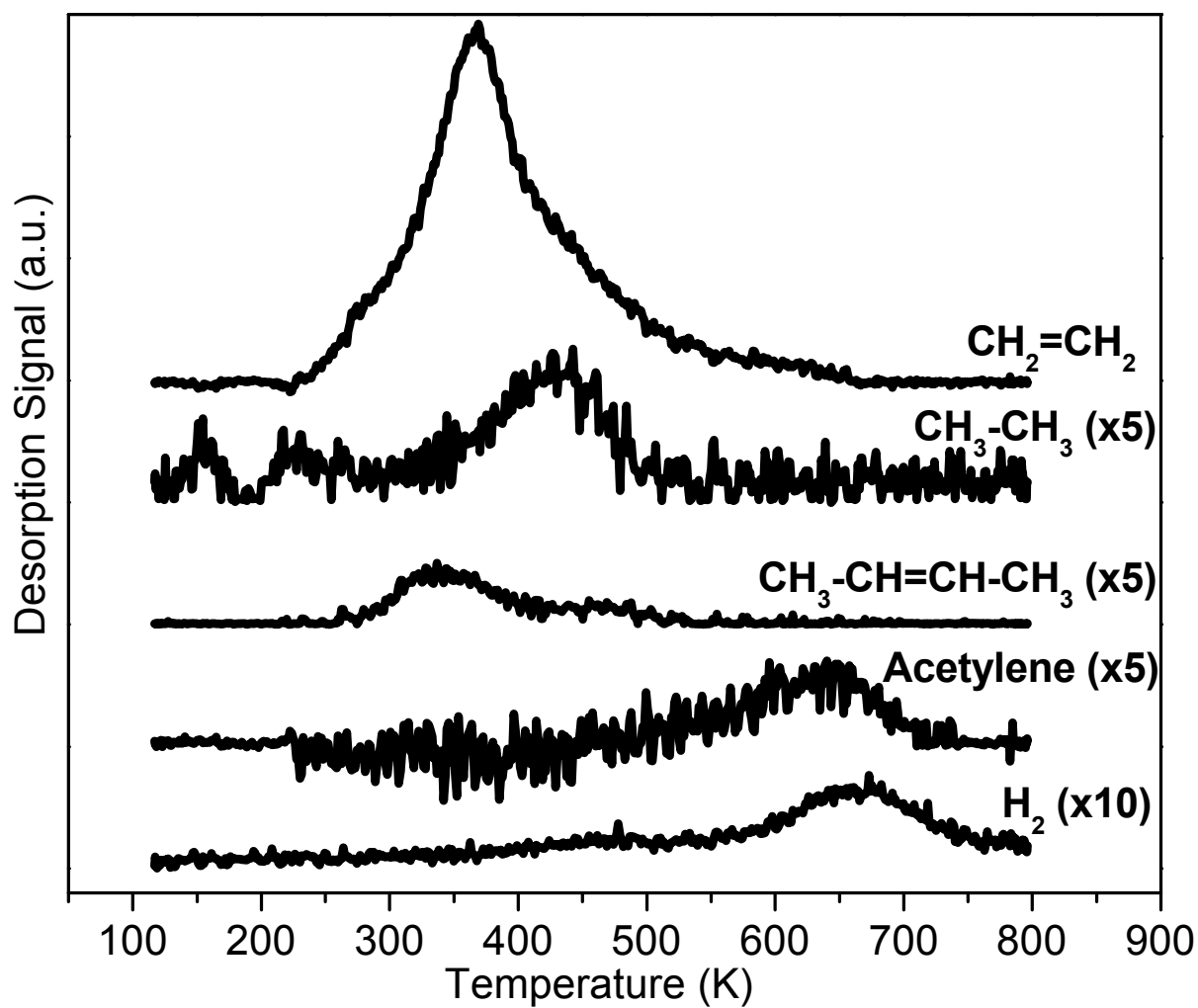
Figure 9. TPD following the first 0.27 L dose of CH_3CHCl_2 on the clean, nearly-stoichiometric α-Cr_2O_3 $(10\bar{1}2)$ surface. Note the scale factors applied to the CH_3CH_3, 2-butene, acetylene and H_2 products. The baselines have been offset for clarity.

near 470 K. Note that this trace chemistry occurs in the high temperature tail associated with ethylene desorption. The evolution of CH_3CH_3 and H_2 near 450 K is consistent with previous observations for the reaction of ethyl intermediates on this surface [17], while the chemistry producing acetylene and H_2 near 650 K is consistent with previous observations of the reaction of vinyl fragments [18] on this surface. These products and their associated surface intermediates suggest a reaction pathway from ethylidene at the minority sites initiated by a β-hydrogen elimination (3.3) to form a vinyl fragment, followed by a α-hydrogen addition (3.4) to another ethylidene surface fragment to form an ethyl fragment.

$$CH_3CH=_{(ads)} \rightarrow CH_2=CH-(ads) + H_{(ads)} \qquad (3.3)$$

$$CH_3CH=_{(ads)} + H \rightarrow CH_3CH_{2(ads)} \qquad (3.4)$$
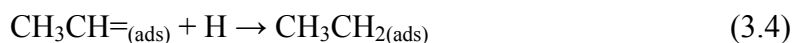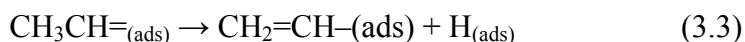
The subsequent chemistry associated with the reaction of ethyl [17] and vinyl [18] intermediates on this surface has been described in detail elsewhere.

The kinetics of 2-butene production in TPD are desorption-limited since the corresponding dosed molecule (not shown) desorbs with a similar looking trace (features at about 470 and 340 K with similar relative peak heights) to that observed following exposure to CH_3CHCl_2 in the present case [51]. Mass spectrometer fragmentation patterns of the reactant CH_3CHCl_2 reactant molecule (not shown) reveal no evidence for $CH_3CH=CHCH_3$, indicating it does not originate as an impurity in the dosed gas, and must therefore be the result from a surface reaction. The surface chemistry giving rise to $CH_3CH=CHCH_3$ can be explained by the coupling of two ethylidene surface fragments (3.5) forming adsorbed $CH_3CH=CHCH_3$. Given the minority nature of this product,

$$2\ CH_3CH=_{(ads)} \rightarrow CH_3CH=CHCH_{3(ads)} \qquad (3.5)$$

it is possible that this coupling reaction occurs on a small number of defect sites which expose Cr cation centers with multiple coordination vacancies that can bind the two coupling ligands [61]. However, the coupling chemistry is also consistent with previous observations on this surface of vinyl coupling to 1,3-butadiene [18] and methylene coupling to ethylene [19,62], both of which are thought to occur via intermediate migration between adjacent cation sites on terraces.

3.2.2. Post-reaction AES

An AES spectrum for the clean surface is shown in Figure 10a, and displays the typical fingerprint of the nearly-stoichiometric α-Cr_2O_3 $(10\bar{1}2)$ surface with Cr and O features in the range of 470-550 eV. Figure 10b displays a post-reaction AES spectrum taken after many sequential CH_3CHCl_2 exposures and TPD runs for an accumulated total dose of 6.5 L (same data as shown in Figure 8), and shows a chlorine feature near 181 eV characteristic of an AES Cl/Cr ratio of 0.32 corresponding to a near monolayer coverage of chlorine adatoms [20]. No surface carbon (272 eV) is observed from the reaction of CH_3CHCl_2 in post-reaction AES measurements (Figure 10b). Narrow scans over the C AES region at S/N ratios a factor of 13 better than those in Figure 10b (not shown) show no evidence of surface carbon, and demonstrates that carbon coverages resulting from our thermal desorption studies are less than 2% ML, and below the detection limits of our AES measurement.

3.2.3. Soft X-ray photoelectron spectroscopy

Figure 11 shows the results of an XPS characterization of adsorbed CH_3CHCl_2 on the nearly-stoichiometric α-Cr_2O_3 $(10\bar{1}2)$ surface. For each spectrum, a freshly-prepared clean sample was exposed to a 100 L dose of CH_3CHCl_2 at 150 K and heated to the
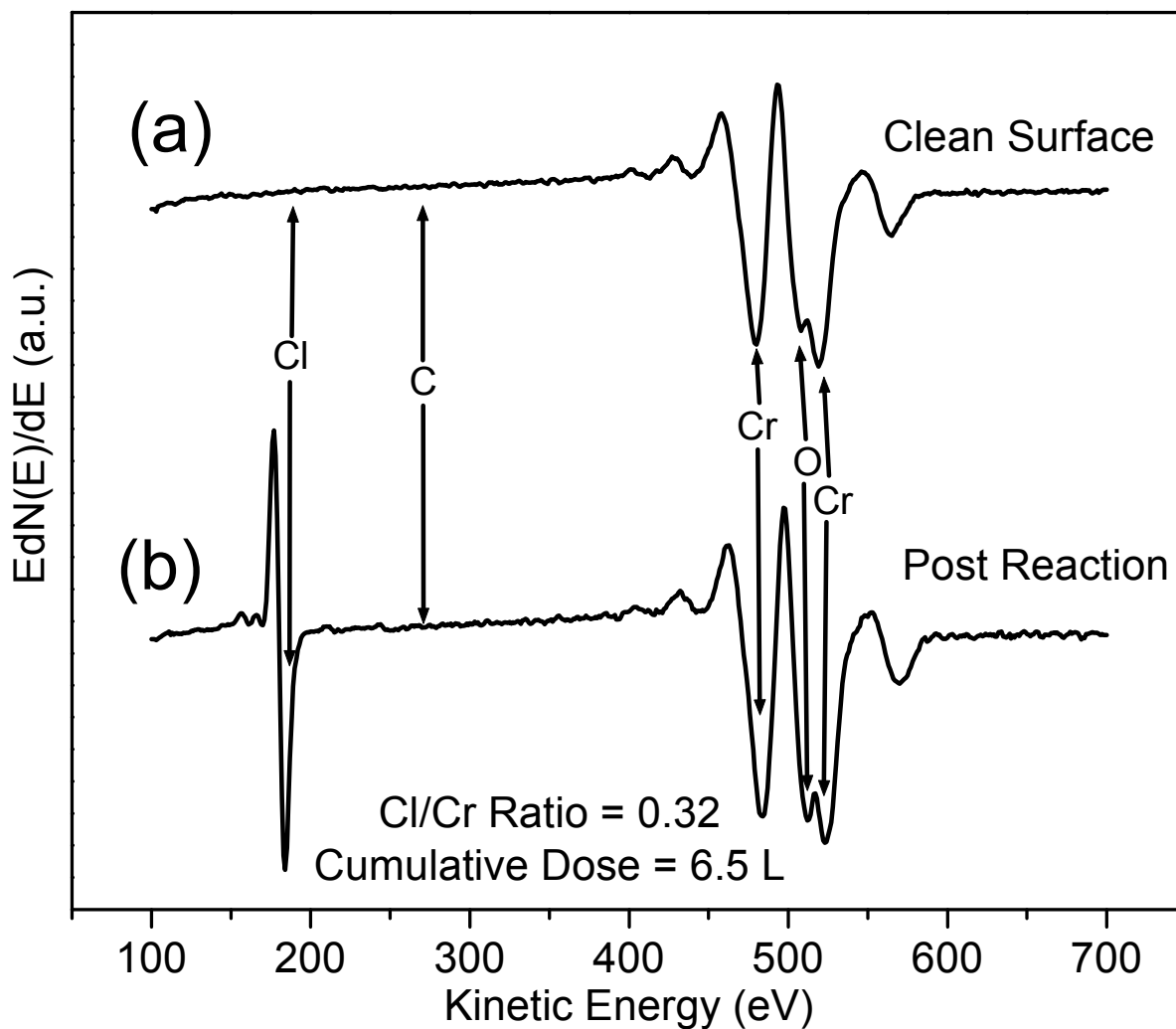
Figure 10. Auger electron spectra (AES) of both (a) clean, nearly-stoichiometric and (b) post-reaction Cl terminated α-Cr_2O_3 $(10\bar{1}2)$ surfaces. Principle Auger electron peak locations are labeled and the Cl/Cr ratio of the post-reaction Cl terminated surface is indicated at the bottom of the plot.
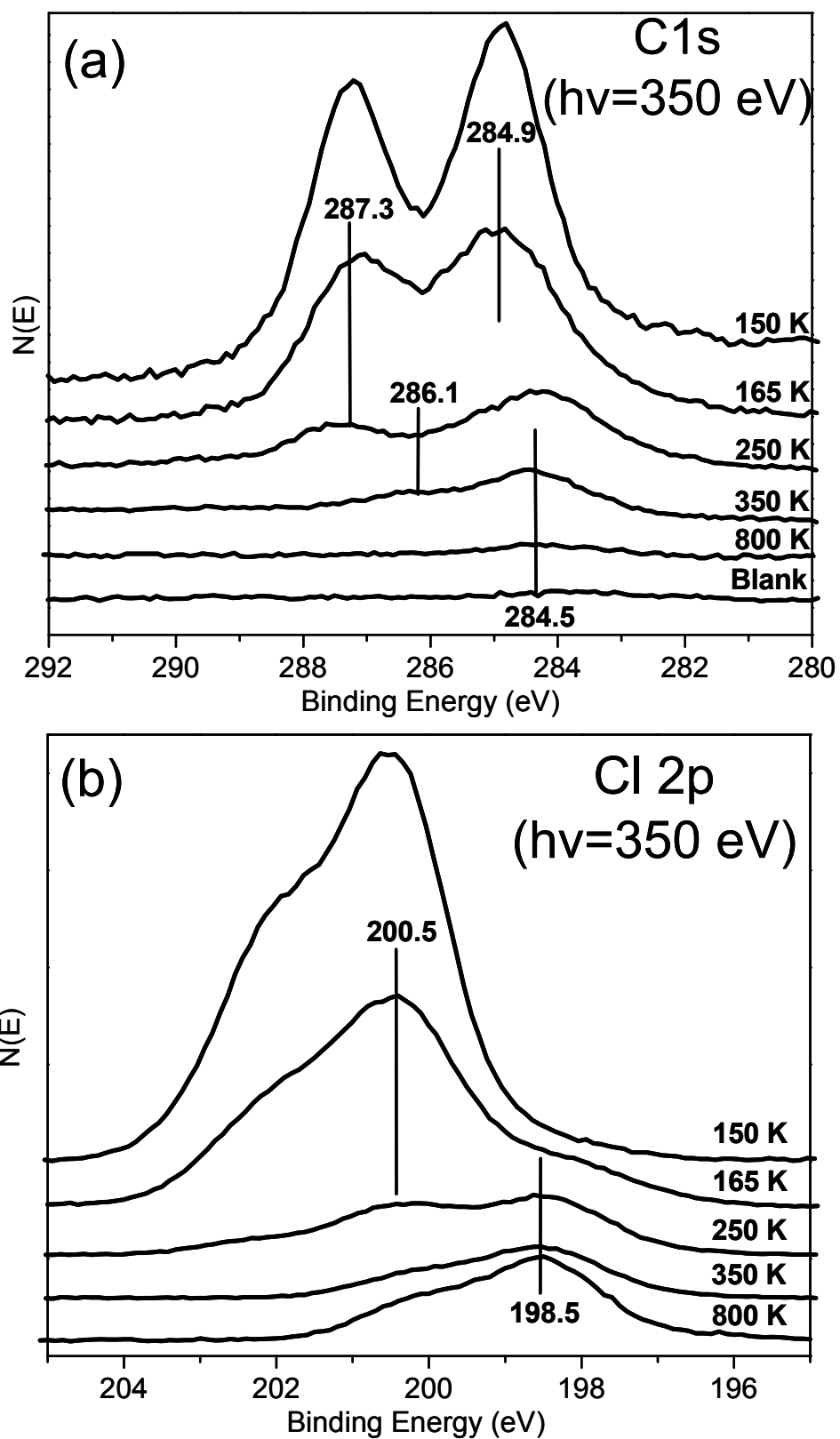
Figure 11. (a) C 1s and (b) Cl 2p XPS spectra collected following 100 L CH_3CHCl_2 exposures at 150 K followed by heating to the temperature shown on the plot. The sample was freshly prepared before each measurement to avoid beam damage.

specified temperature for a period of one minute. Following each heating treatment, the sample was cooled again to near 150 K, and photoemission spectra were collected in an attempt to isolate the surface intermediate(s) formed during the thermally-induced surface reaction of CH_3CHCl_2. The sample was freshly prepared between each measurement in order to avoid beam damage of the adlayer due to excessive exposure to the high flux of synchrotron radiation (350 eV) and the low-energy electrons (0.5 eV) from the flood gun used for charge neutralization.

Figure 11a shows the series of C 1s spectra, and Figure 11b shows the corresponding data for Cl 2p. The C 1s spectrum collected after dosing at 150 K shows two contributions at ~287 and 285 eV attributed to the doubly chlorinated carbon (–$CHCl_2$) and the aliphatic methyl carbon (CH_3–) of molecular CH_3CHCl_2, respectively [33]. As the temperature is increased to 165 K the intensity of the spectrum decreases and the peaks broaden producing less splitting between the features. The decreased intensity is due to desorption of molecular CH_3CHCl_2. The broadening and reduced splitting both point to the possibility of an unresolved, intermediate binding energy feature bracketed by the features near 287 and 285 eV.

Heating to higher temperatures causes an additional drop in intensity of the C 1s spectrum due to the desorption of molecular CH_3CHCl_2, At 250 K a disproportionately larger drop in the high binding energy feature is observed and attributed to C-Cl bond cleavage. After heating to 350 K the high binding energy (287 eV) feature is essentially gone, indicating that molecular CH_3CHCl_2 has either desorbed or dissociated via C-Cl bond cleavage. A small feature at intermediate binding energies (286.1 eV) is observed along with the feature at 284.5 eV. The feature at intermediate binding energies (286.1

eV) is attributed to a singly-chlorinated carbon species by comparison to spectra for ethyl chloride, CH_3CH_2Cl [17]. We assign this signal to the singly-chlorinated carbon in an α-chloroethyl, $CH_3CHCl–$, surface intermediate formed by a single C-Cl bond breaking event.

The larger intensity of the low binding feature (284.5 eV) following heating to 350 K indicates that only a fraction of that feature can be associated with an α-chloroethyl intermediate. This binding energy is consistent with alkyl carbon, and the additional intensity is attributed to the ethylidene ($CH_3CH=$) surface intermediate suggested by the TPD results and expected for complete C-Cl bond breaking in CH_3CHCl_2. The C 1s binding energy of 284.5 eV indicates that the ethylidene is bound to surface Cr cations rather than O anions following C-Cl bond cleavage since C 1s binding energies for oxygenated carbons (ex., alkoxides, carboxylates, carbonates) typically fall at binding energies of 286 eV or greater [33,55]. However, because of the presence of the intermediate binding energy feature at 286.1 eV attributed to a chlorinated surface intermediate, we can not definitely rule out the possibility of an ethylidene surface species with a single C-O bond (ex., bridged between neighboring surface Cr cations and O anions).

Heating to 800 K removes the majority of the surface carbon, consistent with the evolution of carbon-containing reaction products in this temperature range in TPD. In contrast to post-reaction AES results, a small amount of surface C remains after heating to 800 K. This difference is thought to be due to uptake of residual background gas in the chamber from the multiple 100 L exposures of CH_3CHCl_2 using the backfill method. A

similar amount of surface-carbon is observed at the same binding energy as that of the 800 K spectrum from a blank without any deliberate exposure to CH_3CHCl_2.

The Cl 2p spectra shown in Figure 11b exhibit a similar trend to the C 1s data. Higher binding energy Cl 2p features are observed following the dose, and the higher binding energy features are lost as a result of heating. The Cl 2p spectrum collected after the dose at 150 K is characteristic of a partially-resolved Cl 2p doublet with a Cl $2p_{3/2}$ binding energy of 200.5 eV. Heating to temperatures up to 350 K results in a decrease and eventual loss of the high binding energy features, and leaves a contribution primarily associated with a single, partially resolved Cl 2p doublet with a Cl $2p_{3/2}$ feature at 198.5 eV. Similar to the assignment for C 1s, the high binding energy features are attributed to Cl associated with intact C-Cl bonds (molecular CH_3CHCl_2 or CH_3CHCl–), with the low binding energy features attributed to a Cl adatom surface reaction product. This low binding energy of the remaining Cl 2p doublet (Cl $2p_{3/2}$ at 198.5 eV) is characteristic of metal chloride [33], and is assigned to Cl adatoms bound at surface Cr sites, consistent with earlier reports of the capping of surface Cr cations by halogen adatoms [17,18,20,21].

3.3 Discussion

3.3.1. Initial dissociation

The thermal decomposition of 1,1-dichloroethane on α-Cr_2O_3 ($10\bar{1}2$) results in surface Cl adatoms, surface ethylidene and α-chloroethyl fragments. XPS results suggest C-Cl bond cleavage can proceed in a sequential fashion since the presence of singly chlorinated carbons is observed in XPS following large doses of 1,1-dichlorethane. Since desorption of the 1,1-dichloroethane reactant is only observed from small doses in TPD

after the build up surface Cl, it is likely that this sequential dissociation process occurs primarily on partially chlorinated regions of the surface, with complete dissociation requiring multiple cation sites to accommodate the organic ligand and the two Cl atoms.

3.3.2. CH$_3$CHCl$_2$ desorption

The highest temperature CH$_3$CHCl$_2$ desorption feature in TPD at 410 K is likely due to recombination of α-chloroethyl fragments on the surface with Cl adatoms deposited from C-Cl bond cleavage, with the lower temperature CH$_3$CHCl$_2$ desorption feature attributable to desorption of a molecular surface species. The recombination peak exhibits first-order kinetics since the peak temperature is invariant with coverage, despite the fact that recombination would typically be considered a second-order elementary process to combine the α-chloroethyl fragment with a Cl atom to produce the CH$_3$CHCl$_2$ desorption product. Therefore, the rate-limiting step must be a first-order process associated with either the availability of Cl atoms or α-chloroethyl fragments, possibly associated with diffusion of one of the species. The activation barrier for the process is 26 kcal/mol based on a Redhead analysis [52], assuming a normal first-order pre-exponential factor of 10^{13} s^{-1}.

3.3.3. Mechanism for the intramolecular isomerization of ethylidene to ethylene

Scheme 1 shows possible pathways for the intramolecular isomerization reaction (3.2) required to produce the CH$_2$=CH$_2$ product from the proposed ethylidene intermediate. The upper path represents a rate-limiting, first-order desorption of the ethylidene intermediate followed by first-order, intramolecular isomerization in the gas phase to the CH$_2$=CH$_2$ product. The lower pathway represents a rate-limiting, first-order, surface- bound intramolecular isomerization of ethylidene to an ethylene species,
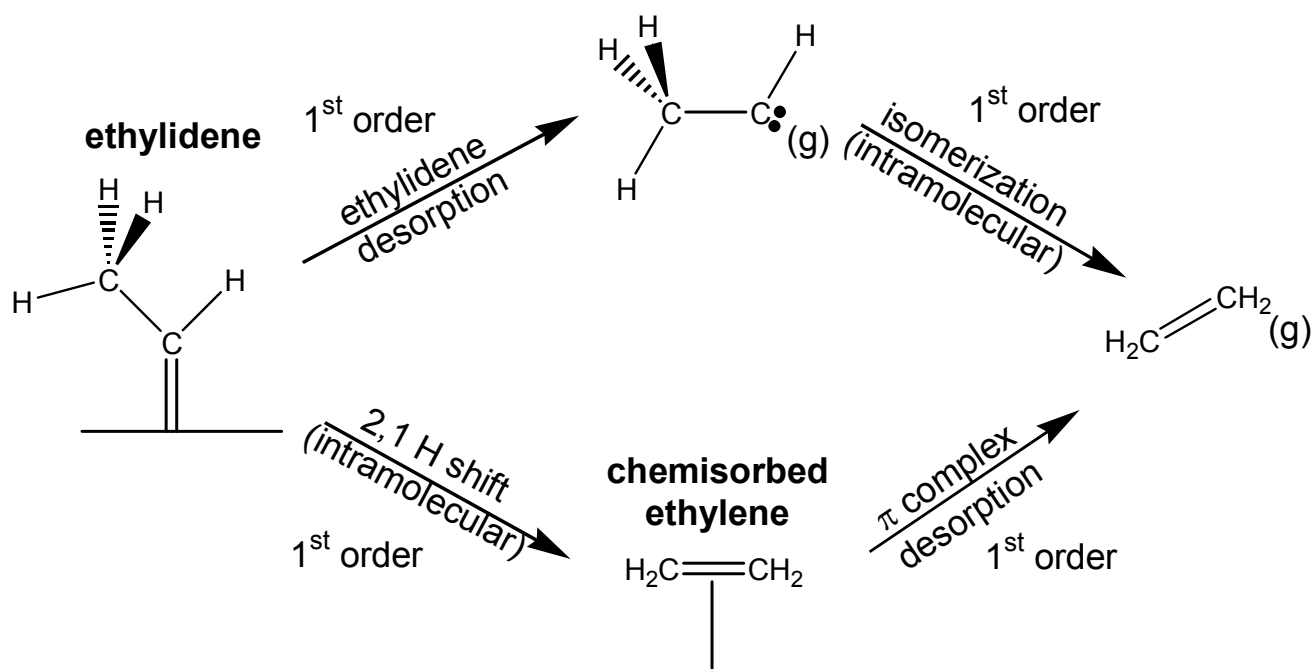
Scheme 1. Possible routes from ethylidene to gas-phase $CH_2=CH_2$. The top route represents the desorption and gas-phase isomerization of ethylidene, while the middle and bottom routes represent possible surface mediated routes to $CH_2=CH_2$.

followed by desorption of that ethylene species to the gas-phase.

The gas-phase, first-order, intramolecular isomerization to $CH_2=CH_2$ shown in the upper path of Scheme 1 has been studied theoretically [63]. Nonemperical LCAO-MO-SCF calculations with a double ζ basis set predicts an activation barrier of 20.9 kcal/mol for the isomerization process between the singlet ground states of each species [63] which is comparable to the activation barrier of 24 kcal/mol obtained in our TPD experiments. However, there is no evidence in the literature for ethylidene desorption from other surfaces. In contrast, methyl (CH_3-) desorption has been observed on Cu(111) [64,65], Ni(100) [66], Ag(111) [67] and O/Mo(110) [68], and methylene ($CH_2=$) desorption has been observed from an Al surface [69]. In each of these cases, the gas-phase species (methyl or methylene) was identified by mass spectrometer fragmentation patterns, where the parent mass was clearly an unsaturated hydrocarbon species. In the case of ethylidene, the parent mass is the same as that of the $CH_2=CH_2$ product. Therefore, identification of ethylidene in the gas-phase must rely on distinguishable mass spectrometer fragmentation patterns for ethylidene and $CH_2=CH_2$. Unfortunately, no fragmentation pattern for gas-phase ethylidene is available for comparison. Despite the lack of a clear experimental identification of gas-phase ethylidene, the gas-phase intramolecular isomerization remains a viable pathway. If the activation barrier to ethylidene desorption is higher than the activation barrier to isomerization in the gas-phase, then it is possible that the ethylidene would never be observed in the gas phase before isomerization to $CH_2=CH_2$ product.

The rate-limiting step for the lower pathway in Scheme 1 is the intramolecular 2,1 hydrogen shift reaction to $CH_2=CH_2$ since desorption-limited ethylene evolves at 290 K

[51], well below the 385 K reaction temperature in TPD. A similar 2,1-hydrogen shift reaction has been proposed for the conversion of vinylidene to acetylene in previous work on the $(10\bar{1}2)$ surface [21]. On Pt (111) [13] the 2,1-H shift has been observed in competition with α-elimination to ethylidyne species. The 2,1-hydrogen shift has also been proposed for a variety of systems with an alkylidene bound at a metallic site. In a study on the initiation of ethylene polymerization on Cr/Silica catalyst [70], the 2,1-hydrogen shift was suggested as the termination step for the polymerization process. Theoretical and experimental studies of iron carbene complexes reveal that the 2,1-H shift reaction is very favorable [71,72]. Therefore, based on precedence from the literature as well as previous chemistry observed on the α-Cr$_2$O$_3$ $(10\bar{1}2)$ [21], the surface-mediated intramolecular isomerization of ethylidene to CH$_2$=CH$_2$ is considered the most likely reaction pathway to ethylene from ethylidene.

3.3.4. Activity of α-Cr$_2$O$_3$ $(10\bar{1}2)$

The Cl adatoms deposited on the nearly-stoichiometric α-Cr$_2$O$_3$ $(10\bar{1}2)$ surface during the reaction of CH$_3$CHCl$_2$ have a significant impact on the activity of the surface. The observed binding energy of the Cl adatoms in XPS is consistent with a metal chloride, and indicates that Cl adatoms block active Cr^{3+} sites for the reaction, consistent with earlier reports [17,18]. In the catalysis literature, deactivation of powdered Cr$_2$O$_3$ catalysts has been attributed to carbon deposition [57], and to the formation of inactive crystalline phases at the surface that isolate cations from the surface [58]. In this work, no new crystalline phases are observed as a result of reaction; the LEED pattern (not shown) retains the (1×1) periodicity of the nearly stoichiometric surface. Likewise, no carbon residue is deposited on the α-Cr$_2$O$_3$ $(10\bar{1}2)$ surface as a result of the reaction of

ethylidene under the conditions of our experiments. These results suggest that under the conditions of this study ethylidene fragments are not a major intermediate in coke production on $(10\bar{1}2)$ facets, where the available cation and anion sites expose primarily a single coordination vacancy.

3.4 Conclusions

The reaction of ethylidene species was investigated on the nearly-stoichiometric α-Cr_2O_3 $(10\bar{1}2)$ surface under UHV conditions via the dissociative adsorption of CH_3CHCl_2. The reaction primarily yields $CH_2=CH_2$; however, trace amounts of acetylene, CH_3CH_3, H_2 and $CH_3CH=CHCH_3$ were also observed. The rate-limiting surface reaction step for the primary chemistry producing $CH_2=CH_2$ is an intramolecular isomerization (2,1-hydrogen shift) from an ethylidene intermediate. Chlorine adatoms from the dissociation of CH_3CHCl_2 deactivate the surface by simple Cr cation site blocking. No surface carbon is observed in post reaction surface analysis, indicating that under the conditions of this study ethylidene species are likely not primary coke forming intermediates on $(10\bar{1}2)$ facets of α-Cr_2O_3.

Chapter 4

Reactions of ethylidyne groups on a model chromia surface: 1,1,1-Trichloroethane on stoichiometric α-Cr$_2$O$_3$ (10$\bar{1}$2)

4.1 Introduction

Supported chromia catalyst are used industrially in the catalytic dehydrogenation of C$_3$ and C$_4$ alkanes [2], and a number of studies have examined the applicability of chromia catalysts to the dehydrogenation and oxidative dehydrogenation of ethane [4-8]. In this study, the reactions of ethylidyne (CH$_3$C$\equiv$) fragments are examined over a model chromia single crystal surface, α-Cr$_2$O$_3$ (10$\bar{1}$2). Previous work with this model system examined both ethyl [17] and ethylidene [18] species as primary and secondary C$_2$-alkyl reaction intermediates, respectively, expected from ethane by C-H bond cleavage from ethane on the same carbon. Ethylidyne species are of interest as the tertiary C$_2$-alkyl reaction intermediate in the same series. For this study, surface ethylidyne species are generated via the thermal dissociation of 1,1,1-trichloroethane.

Stable ethylidyne species have been examined because of their relevance to coke formation from ethylene on metal surfaces [13,40,73-95], oxide supported metals [96-102] and carbide modified metal surfaces [103-107]. By far, the most common means of producing ethylidyne species is by decomposition of di-σ bonded ethylene [73,76,78-80,83,84,86,88-93,95-101,103-108]; however, some groups have also produced ethylidyne by acetylene decomposition [84], hydrogenation of carbon overlayers [77,109] or CO [109], or by decomposition of various halo-hydrocarbon molecules such as 1,1,1-trichloroethane [110], iodoethane [40,102], 1,1-diiodoethane [13], or diiodomethane [77]. Vibrational spectroscopies or photoemission are typically used to identify the stable

ethylidyne surface fragment, and a combination of desorption studies and surface compositional analysis has been utilized to examine reactivities. To our knowledge, all previous studies over model surfaces in ultra high vacuum (UHV) without the presence of excess hydrogen have found that ethylidyne decomposes by both dehydrogenation and C-C bond cleavage leading to carbonaceous overlayers and H_2 desorption. The current work marks a sharp contrast from previous experience with ethylidyne species on model surfaces: no surface carbon deposition is observed and all ethylidyne surface species evolve to gas-phase, hydrocarbon products. To our knowledge, this work is also the first examination of ethylidyne chemistry over a model, metal-oxide surface.

4.2 Results

4.2.1. Reaction products

TPD, AES and XPS reveal that CH_3CCl_3 reacts primarily to acetylene (HC≡CH), ethylene (CH_2=CH_2), H_2 and chlorine adatoms on α-Cr_2O_3 ($10\bar{1}2$); however, trace quantities of vinyl chloride (CH_2=CHCl) and 2-butyne (CH_3−C≡C−CH_3) are also observed. As described below, the selectivity of the reaction is dependent on the Cl adatom coverage. As a result, the reaction was studied primarily using small gas exposures so that variations in reactivity can be related to the extent of Cl deposition.

Gas phase products were identified by comparison of mass spectrometer fragmentation patterns to TPD peak intensities. The relative intensities of four m/z signals were used to identify CH_3CCl_3 (61, 63, 97, 99), HC≡CH (26, 25, 24, 13), CH_2=CH_2 (27, 26, 25, 24), CH_2=CHCl (62, 64, 27, 26) and 2-butyne (54, 53, 39, 50). Overlap of mass signals from 1,1,1-trichloroethane, acetylene, ethylene, vinyl chloride and 2-butyne was accounted for by subtracting overlapping contributions out of the raw

mass spectrometer signal. Following these subtractions, the relative intensities of m/z fragments for all hydrocarbon products formed were found to be in good agreement with mass spectrometer cracking patterns of hydrocarbon standards. Other products were excluded by a search that included m/z values ranging from 2 to 200. Specifically, no CO, CO_2, HCl, Cl_2, or any other oxygenated molecules, halogenated compounds or coupling products were produced from the reaction of CH_3CCl_3 over the nearly-stoichiometric $(10\bar{1}2)$ surface. The lack of oxygenated products is an indication of the nonreducible nature of the surface. No surface carbon was detected with AES following CH_3CCl_3 decomposition; only chlorine was observed as a residual surface reaction product. All desorption traces and quantities have been corrected for mass spectrometer sensitivity.[9]

4.2.1.1. Primary chemistry: acetylene, ethylene and dihydrogen production

Figure 12 shows TPD traces for HC≡CH, $CH_2=CH_2$ and H_2 (the primary reaction products) and the 1,1,1-trichloroethane reactant produced from a 0.44 L ($1L \equiv 1x10^{-6}$ torr·sec) dose at 90 K on a *partially chlorinated* surface. The partially chlorinated surface was produced by two prior 0.44 L doses and TPD runs on an initially clean surface. As determined by AES (below), this treatment results in a Cl coverage of ~ 0.4 ML.[10] Because of the high molecular weight of trichloroethane (MW=133.4), a 0.44 L exposure corresponds to 10% of monolayer coverage.[11]

---

[9] Relative mass spectrometer sensitivity factors of 0.055 for 1,1,1-trichloroethane (m/z 61), 0.67 for acetylene (m/z 26), 0.41 for ethylene (m/z 27), 4.3 for dihydrogen (m/z 2), 0.64 for vinyl chloride (m/z 62) and 0.41 for 2-butyne (m/z 54) were determined experimentally.

[10] 1 ML is defined as one adatom or molecule per surface Cr cation.

[11] Estimates of 1,1,1-trichloroethane coverages are calculated assuming a unity sticking coefficient at 90 K and a total Cr surface site density of $7.5x10^{14}$ Cr/cm^2.
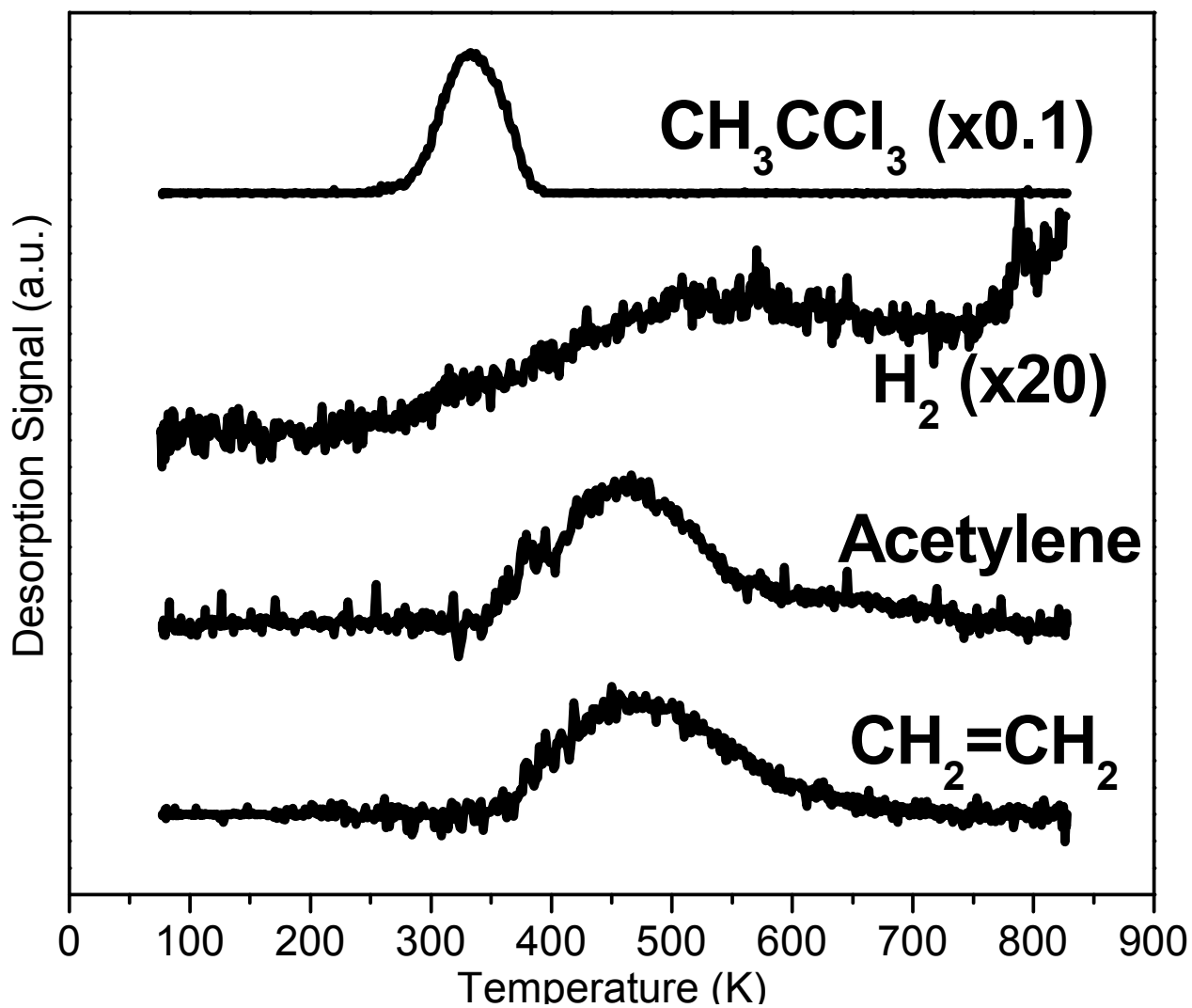
Figure 12. TPD of primary desorption products following the third 0.44 L dose of CH_3CCl_3 on the *partially chlorinated* α-Cr_2O_3 ($10\bar{1}2$) surface. The baselines have been offset for clarity.

All desorbing species evolve between 200 and 700 K. The CH_3CCl_3 reactant molecule desorbs at about 330 K while the primary hydrocarbon reaction products $HC{\equiv}CH$ and $CH_2{=}CH_2$ desorb at 460 and 475, respectively. The hydrocarbon product desorption is accompanied by a broad H_2 desorption profile extending from 300 to 700 K. The presence of an H_2 desorption signal indicates that H-elimination reactions take place under these reaction conditions. Previous work on this surface with ethyl [17] and vinyl [18] species demonstrates that H-elimination reactions are accompanied by H_2 desorption.

The kinetics of the $HC{\equiv}CH$, $CH_2{=}CH_2$ and H_2 traces in Figure 12 are reaction-limited since the corresponding dosed molecules desorb at 310 [21], 290 [51] and 285 K [21], respectively. The presence of all three primary reaction products in the same temperature envelope is an indication that $HC{\equiv}CH$, $CH_2{=}CH_2$ and H_2 originate from a common surface intermediate with the same rate-limiting surface reaction step. The reaction order of the product peaks is not obvious by qualitative inspection of the shapes in Figure 2. However, a variety of coverages were examined using 1,1,1-trichloroethane doses ranging from 0.2 to 4.4 L (not shown), and the temperature maximum of the product peaks remains essentially constant for widely varying amounts of the respective products produced. Therefore, the kinetics of the rate-limiting surface reaction step for hydrocarbon product production is thought to be first order [52]. The apparent first-order activation energy of the surface reaction producing the dominant reaction product, $HC{\equiv}CH$, at 460 K is 29 kcal/mol based on the Redhead analysis [52] and assuming a normal first-order preexponential factor of 10^{13} s^{-1}.

The surface chemistry giving rise to HC≡CH, CH_2=CH_2 and H_2 is readily explained by the presence of an ethylidyne fragment formed from the dissociative adsorption of CH_3CCl_3 (4.1). The presence of H_2 indicates a H-elimination reaction liberating H atoms to the surface. There are no α-hydrogens available in an ethylidyne fragment; therefore, the rate-limiting reaction step is β-hydrogen elimination from ethylidyne to form vinylidene (4.2). Previous work on the $(10\bar{1}2)$ surface demonstrates that vinylidene isomerizes intramolecularly to HC≡CH (4.3) at about this same temperature [21]. Hydrogen freed from the initial β-elimination step is then free to insert into remaining ethylidyne fragments by α-hydrogen addition to form ethylidene (4.4), or couple to form H_2 (4.5). Previous studies of 1,1-dichloroethane on the $(10\bar{1}2)$ surface demonstrate that ethylidene isomerizes intramolecularly to CH_2=CH_2 (4.6) at 385 K [18].

$$CH_3CCl_3 \rightarrow CH_3C\equiv_{(ads)} + 3Cl_{(ads)} \qquad\qquad (4.1)$$

$$CH_3C\equiv_{(ads)} \rightarrow CH_2=CH_2=_{(ads)} + H_{(ads)} \qquad \text{(Rate-limiting step)} \quad (4.2)$$

$$CH_2=CH_2=_{(ads)} \rightarrow HC\equiv CH_{(g)} \qquad\qquad (4.3)$$

$$CH_3C\equiv + H_{(ads)} \rightarrow CH_3CH=_{(ads)} \qquad\qquad (4.4)$$

$$2H_{(ads)} \rightarrow H_{2(g)} \qquad\qquad (4.5)$$

$$CH_3CH=_{(ads)} \rightarrow CH_2=CH_{2(g)} \qquad\qquad (4.6)$$
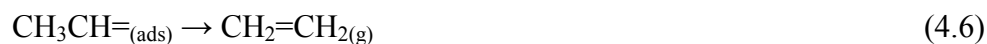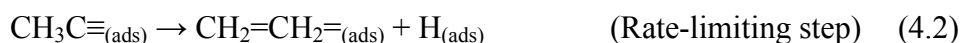
For a series of consecutive 0.44 L exposures of CH_3CCl_3 started on a clean surface, Figure 13 shows integrated TPD peak areas of the desorption traces representing the amount of each desorbing species (corrected for mass spectrometer sensitivity[9]) on the left-hand axis (solid symbols), plotted with the corresponding AES Cl/Cr ratio measured following each TPD run on the right-hand axis (hollow symbols), as a function of the total (cumulative) CH_3CCl_3 exposure. As the cumulative exposure to CH_3CCl_3
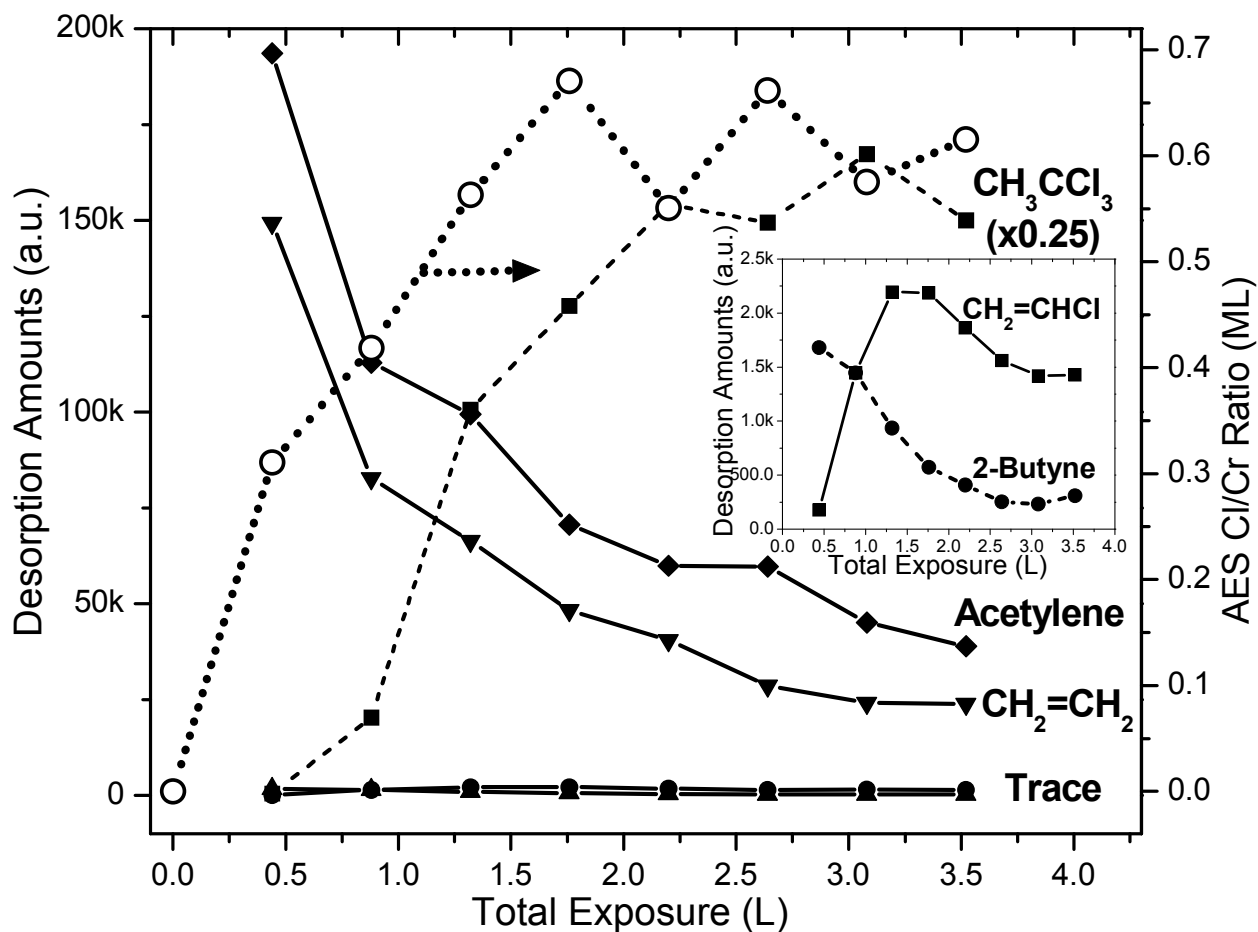
Figure 13. Variation in the relative hydrocarbon desorption amounts for consecutive 0.44 L doses of CH_3CCl_3 on the nearly-stoichiometric α-Cr_2O_3 $(10\bar{1}2)$ surface (solid symbols). Corresponding Cl/Cr ratios are also displayed on the right-hand axis (hollow symbols) scaled so that unity represents 1 Cl adatom per surface Cr cation. The inset shows the trace products for clarity.

increases, the AES Cl/Cr ratio increases, indicating that Cl adatoms are deposited on the surface by dissociative adsorption of CH_3CCl_3. Details of Cl adatom coverage estimates are described elsewhere [20].

Figure 13 shows that the Cl coverage increases most rapidly for total CH_3CCl_3 exposures below 0.9 L and levels off after a total exposure of around 1.3 L. The amounts of the primary reaction products, $HC{\equiv}CH$ and $CH_2{=}CH_2$, steadily decrease and begin to level off towards the end of the range of exposures examined where the product amounts represent less than 20% of the amounts from the initial exposure and TPD run. The amount of unreacted CH_3CCl_3 shows the opposite trend, reacting away completely in the initial run then rising slowly and leveling off coincident with the increasing Cl coverage. The rise in the amount of unreacted CH_3CCl_3 coincident with the decrease in the primary reaction products indicates that the reaction probability decreases with increasing Cl coverage on the surface. The decreased surface reactivity for total CH_3CCl_3 exposures above 1.3 L indicates that Cl adatoms block the active Cr^{3+} sites for the reaction as demonstrated previously [17-21,62].

4.2.1.2. Trace chemistry: 2-butyne and vinyl chloride production

The inset of Figure 13 shows the amounts of the trace products, vinyl chloride and 2-butyne, produced as a function of consecutive dose. Less than 2% of all the reacting CH_3CCl_3 forms these trace products. The amounts of $CH_2{=}CHCl$ and 2-butyne behave differently with the increasing Cl coverage on the surface. For the initial 0.44 L exposure of CH_3CCl_3, when the Cl coverage on the surface is a minimum, no $CH_2{=}CHCl$ is observed and the 2-butyne product is at a maximum. As the Cl coverage increases, the amount of 2-butyne decreases. The amount of $CH_2{=}CHCl$ shows an initial enhancement,

53

reaching a maximum for a total CH_3CCl_3 exposure of 1.3 L, then steadily decreases and levels off throughout the remaining exposures examined. The contrasting behavior of the trace products suggests a different relationship between the chemistry producing the trace products and the Cl adatoms deposited from dissociative adsorption of CH_3CCl_3.

The initial enhancement of CH_2=CHCl production appears to be related to the initial Cl adatom deposition, while the subsequent decline in reactivity appears to be related to Cl adatom site blocking of the majority of reactive surface sites. Additionally, the CH_3CCl_3 desorption product is only observed in TPD after the buildup of surface chlorine, indicating that the dissociation reaction is inhibited by Cl deposition. The behavior of these chlorinated desorption products suggests that the CH_2=CHCl product may be due to the partial dissociation of CH_3CCl_3 on partially chlorinated regions of the surface, since complete dissociation requires multiple vacant cation sites to accommodate the organic ligand and three Cl adatoms.

Figure 14 shows TPD traces for CH_2=CHCl (Figure 14a) and 2-butyne (Figure 14b) from the third and first 0.44 L exposures and TPD runs of CH_3CCl_3, respectively. The CH_2=CHCl feature in Figure 14a evolves at 380 K. The kinetics of CH_2=CHCl are reaction-limited since dosed CH_2=CHCl evolves at 280 K [18]. Mass spectrometer fragmentation patterns of the CH_3CCl_3 reactant molecule (not shown) reveal no evidence for CH_2=CHCl, indicating that this species is not an impurity in the dosed gas. To obtain CH_2=CHCl from CH_3CCl_3 two things must occur: the chlorinated carbon must lose two Cl atoms and one hydrogen atom must migrate from the methyl carbon to the chlorinated carbon. The loss of two Cl atoms relative to the CH_3CCl_3 reactant, as well as the relationship between the reactivity of the surface towards CH_2=CHCl production and Cl

54
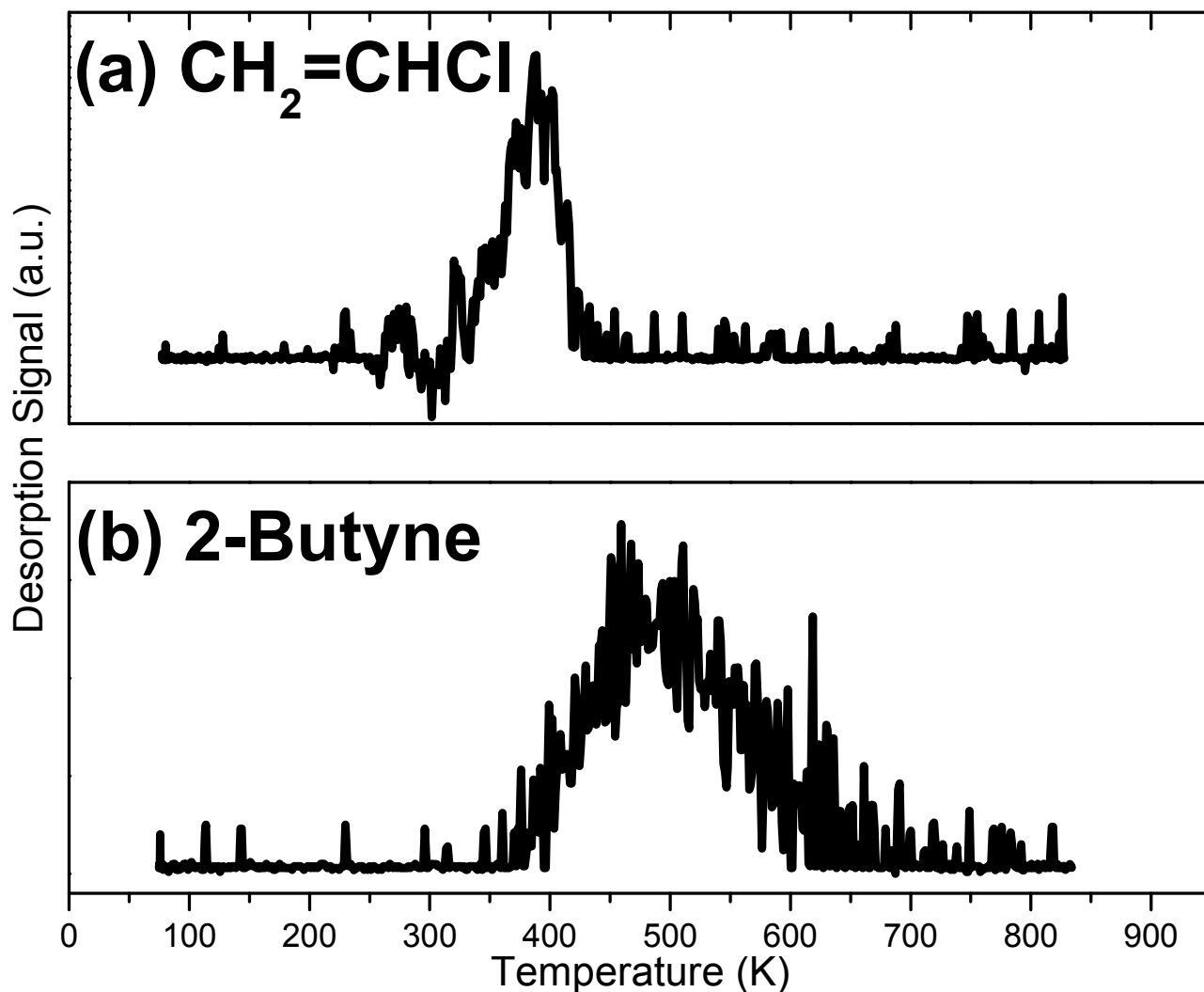
Figure 14. TPD of trace reaction products following 0.44 L exposures of CH_3CCl_3 on the α-Cr_2O_3 ($10\bar{1}2$) surface for (a) CH_2=CHCl following the third exposure on the *partially chlorinated* surface and (b) 2-butyne following the initial exposure on the clean surface.

adatom deposition, suggests the reactive intermediate may be an α-chloroethylidene

fragment from the partial dissociation of CH_3CCl_3 (4.7). Because C-Cl bond cleavage is

typically considered facile [11,56], the rate-limiting step to vinyl chloride production is

most likely the hydrogen atom transfer. Two possible pathways exist for the hydrogen

atom migration: intramolecular (4.8) or surface mediated (4.9). The desorption

$$CH_3CCl_{3(ads)} \rightarrow CH_3CCl{=}_{(ads)} + 2Cl_{(ads)} \qquad (4.7)$$

$$CH_3CCl{=}_{(ads)} \rightarrow CH_2{=}CHCl_{(g)} \qquad (4.8)$$

$$CH_3CCl{=}_{(ads)} \rightarrow CH_2{=}CCl{-}_{(ads)} + H_{(ads)} \rightarrow CH_2{=}CHCl_{(g)} \qquad (4.9)$$
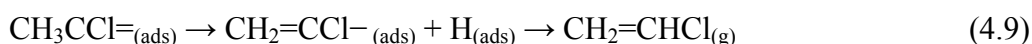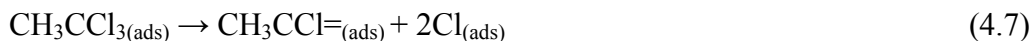
temperature for ethylene from the intramolecular isomerization of ethylidene on the α-

Cr_2O_3 (10$\bar{1}$2) surface [18] is 385 K, similar to the temperature observed for $CH_2{=}CHCl$

production in the present case. The similar desorption temperatures for the respective

products suggest that intramolecular isomerization (4.8) is the most likely pathway.

However, the broad H_2 desorption profile in Figure 12 beginning at ~300 K prevents us

from ruling out the surface mediated route (4.9).

The 2-butyne feature shown in Figure 14b evolves at 475 K. The kinetics for 2-

butyne are desorption-limited since dosed 2-butyne (not shown) evolves at about this

same temperature [51]. Despite the desorption-limited kinetics, the 2-butyne production

is thought to be due to some surface reaction originating with the CH_3CCl_3 reactant

molecule. A similar circumstance was encountered in previous work on the α-Cr_2O_3

(10$\bar{1}$2) surface where ethylidene fragments couple to 2-butene [18]. Mass spectrometer

fragmentation patterns of the CH_3CCl_3 reactant molecule (not shown) reveal no evidence

for 2-butyne, indicating it does not originate as an impurity in the dosed gas. The surface

chemistry giving rise to 2-butyne at 475 K may be explained by coupling of two

ethylidyne fragments on the surface forming an adsorbed 2-butyne molecule on the

surface (4.10). Given the minority nature of this product, it is possible that this coupling
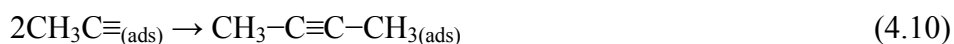
$$2CH_3C\equiv_{(ads)} \rightarrow CH_3-C\equiv C-CH_{3(ads)} \tag{4.10}$$

reaction occurs on a small number of defect sites which expose Cr cation centers with

multiple coordination vacancies that can bind the two coupling ligands [61]. However,

the coupling chemistry is also consistent with previous observations on this surface of

vinyl coupling to 1,3-butadiene [18] and methylene coupling to ethylene [19,62], both of

which are thought to occur via intermediate diffusion between adjacent cation sites on

terraces. In light of these two possibilities, the steady decline of 2-butyne production

coincident with the increasing Cl adatom coverage can either be related to Cl site

blocking of low coordinate, defect Cr centers [18] or blocking of ethylidyne diffusion

pathways across the surface [18,19,62].

4.2.1.3. CH₃CCl₃ defect chemistry

In addition to the chemistry described above, we have observed additional

chemistry that appears to be defect driven during separate experiments on a different α-

Cr_2O_3 $(10\bar{1}2)$ crystal, subjected to years of Ar^+ ion bombardment and annealing

treatments. From this second crystal, $HC\equiv CH$ and H_2 are observed in TPD above 700 K

(not shown) in addition to the chemistry at lower temperatures reported in Figure 2.

These extra features represent less than 0.5% of all reaction products. Additionally, these

extra features have a sharp peak shape and are rapidly poisoned by the deposition of Cl

adatoms from dissociative adsorption, indicating a preferential binding of Cl adatoms to

these active sites. The lack of these TPD features from a crystal subjected to much less

ion bombardment and annealing (Figure 12), as well as the sharp shape, rapid poisoning

and higher temperature indicates a stabilization of ethylidyne species likely because they are bound to defect sites. The lack of this defect related chemistry on the crystal utilized in the TPD experiments of Figure 12 and 13 indicates that the primary chemistry occurs on terrace sites on the α-Cr_2O_3 $(10\bar{1}2)$ surface.

4.2.2. Post-reaction AES

An AES spectrum for the clean surface is shown in Figure 15a, and displays the typical fingerprint of the nearly-stoichiometric α-Cr_2O_3 $(10\bar{1}2)$ surface with Cr and O features in the range of 470-550 eV. Figure 15b displays a post-reaction AES spectrum taken after many sequential CH_3CCl_3 exposures and TPD runs for an accumulated total dose of 3.5 L (same data as shown in Figure 13). The chlorine feature near 181 eV represents a Cl/Cr ratio of 0.2 characteristic of ~60% monolayer coverage of chlorine adatoms. No surface carbon (272 eV) is observed from the reaction of CH_3CCl_3 in post-reaction AES measurements (Figure 15b). Narrow scans over the C AES region at S/N ratios a factor of 13 better than those in Figure 15b (not shown) show no evidence of surface carbon, and demonstrates that carbon coverages resulting from our thermal desorption studies are less than 2% of a ML, and below the detection limits of our AES measurement. The surface O/Cr ratio measured before and after CH_3CCl_3 TPD experiments show no change due to the deposition of surface chlorine. Therefore, no evidence is observed for the replacement of lattice oxygen by chlorine under these experimental conditions.

4.2.3. Soft X-ray photoelectron spectroscopy

Figure 16 shows a C 1s and Cl 2p XPS characterization of adsorbed CH_3CCl_3 on the nearly-stoichiometric α-Cr_2O_3 $(10\bar{1}2)$ surface. For each set of spectra, a freshly
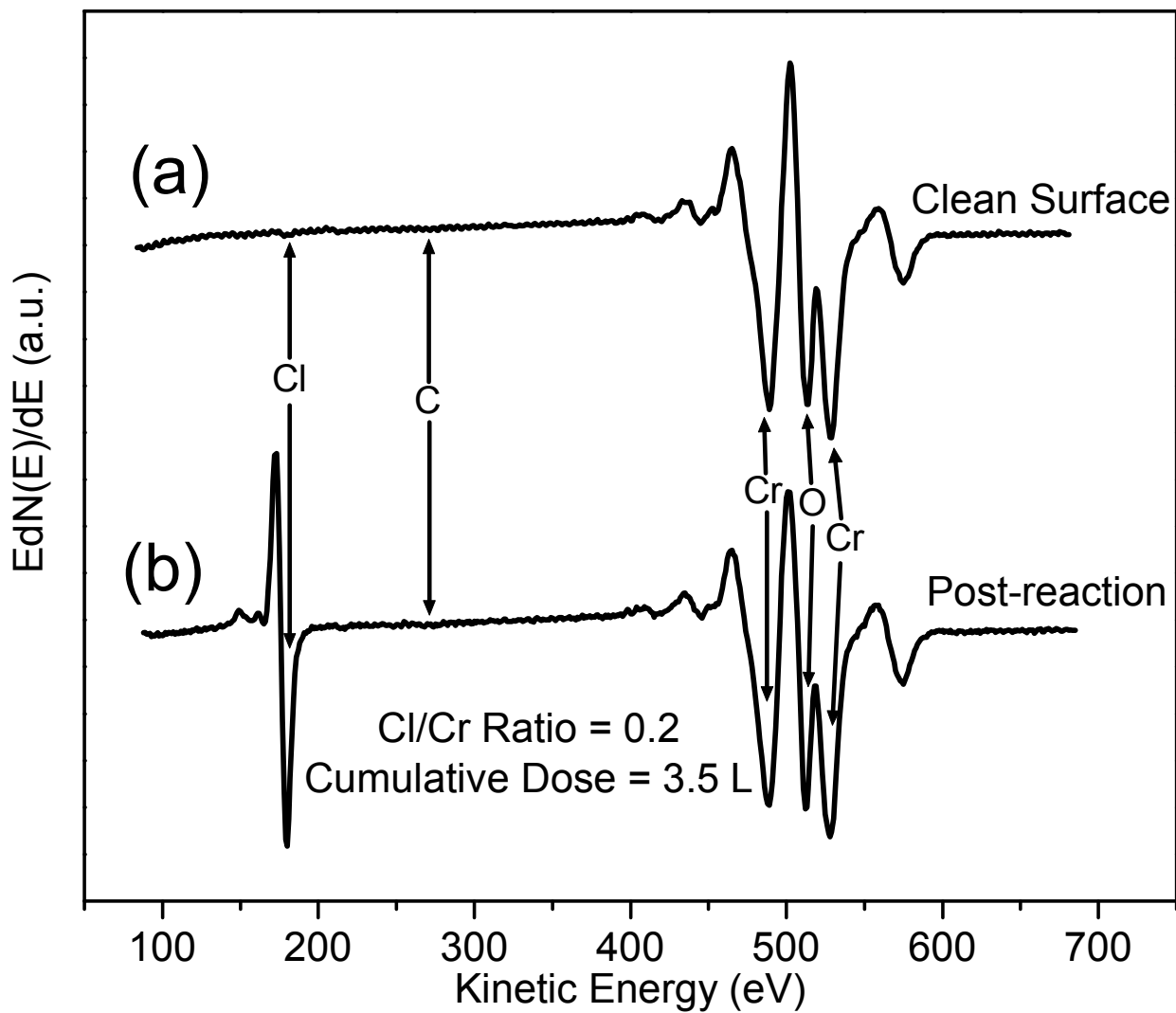
Figure 15. Auger electron spectra (AES) of both (a) clean, nearly-stoichiometric and (b) post-reaction Cl terminated α-Cr$_2$O$_3$ (10$\bar{1}$2) surfaces. Principle Auger electron peak locations are labeled and the Cl/Cr ratio of the post-reaction Cl terminated surface is indicated at the bottom of the plot.
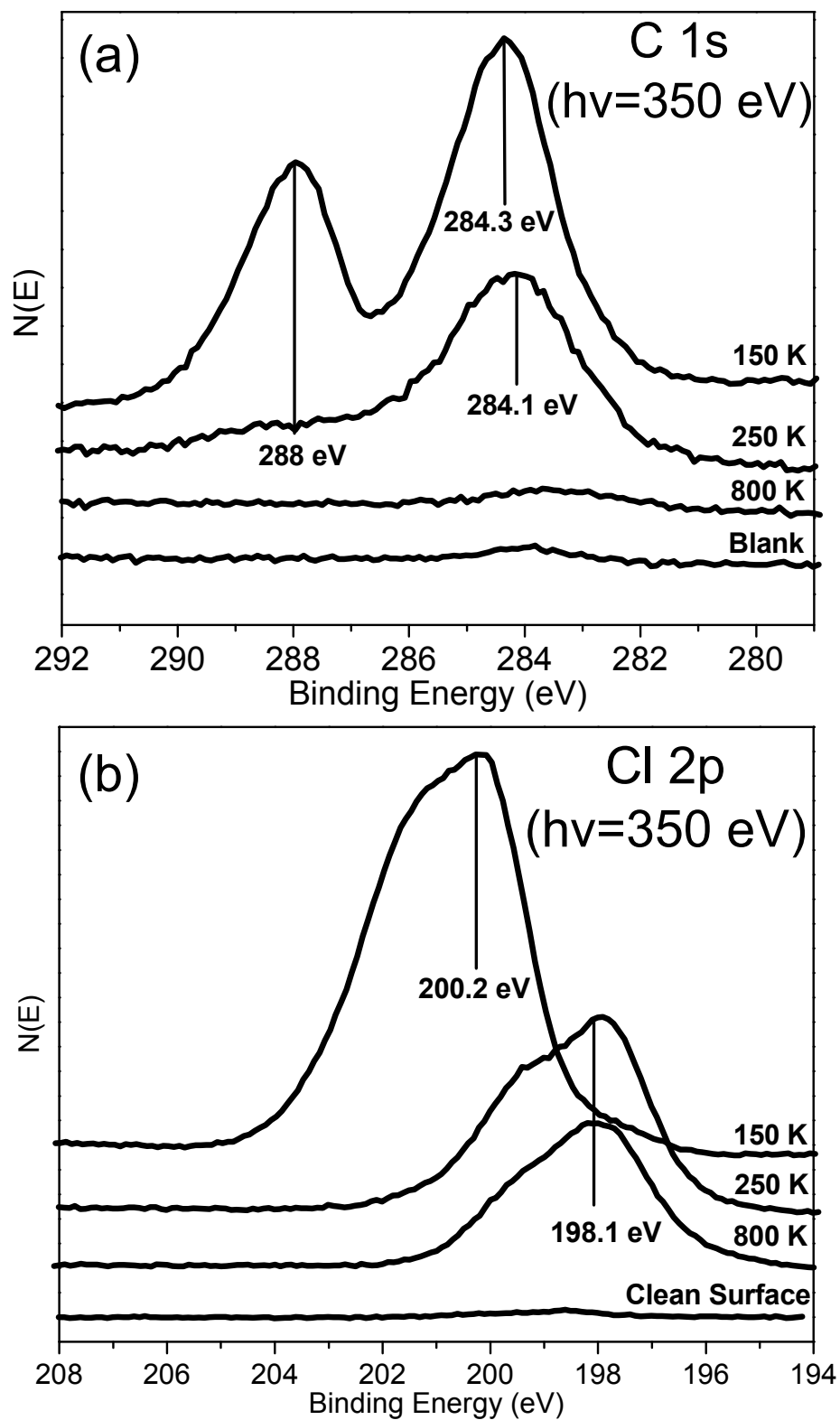
Figure 16. (a) C 1s and (b) Cl 2p XPS spectra collected following a 44 L CH_3CCl_3 exposure at 150 K followed by heating to successively higher temperatures.

prepared sample was exposed to 44 L of CH_3CCl_3 at 150 K and heated to the temperature shown on the plot for a period of a minute. Following each heating treatment, the sample was cooled again to near 150 K and photoemission spectra were collected in an attempt to isolate the surface intermediate formed during the thermally-induced surface reaction of CH_3CCl_3. The sample was freshly prepared between each measurement in order to avoid beam damage in the adlayer due to excessive exposure to the high flux of synchrotron radiation (350 eV) and the low-energy electrons (0.5 eV) from the flood gun used for charge neutralization.

Figure 16a shows the series of XPS C 1s spectra, and Figure 16b shows the corresponding data for Cl 2p. The C 1s spectrum collected after dosing at 150 K shows two contributions at ~284 eV and 288 eV attributed to the methyl carbon (CH_3-) and the triply chlorinated carbon (-CCl_3) of molecular CH_3CCl_3, respectively [81]. Heating the surface to 250 K, causes the intensity of the high binding energy feature to decrease, due to both molecular CH_3CCl_3 desorption and C-Cl bond cleavage. What remains is a peak at 284.1 eV, broadened towards lower binding energy relative to the 150 K spectrum, with a high binding energy tail extending to 288 eV suggesting the possibility of a small, unresolved, intermediate binding energy contribution(s) between 284 and 288 eV. The FWHM for the low binding energy features in the 150 and 250 K spectra are 2.1 and 2.8 eV, respectively. The broadening and slight shift from 284.3 to 284.1 eV of the low binding energy feature upon heating from 150 to 250 K is consistent with the presence of multiple, unresolved C 1s binding energies. These remaining features in the 250 K spectrum are characteristic of the reaction intermediates responsible for the hydrocarbon and chloro-hydrocarbon desorption products observed in TPD above 300 K.

Two XPS characterizations in the literature of adsorbed ethylidyne on Rh (111) [73] and Pt (111) [110] are useful in our assignment of the peaks observed in the 250 K spectrum. Andersen et al. [73] produce ethylidyne fragments on the Rh (111) surface by thermal activation of adsorbed ethylene. Two primary C 1s features are reported at 284.0 and 283.4 eV, assigned to the methyl (CH_3-) end of the fragment and the α-carbon ($-C\equiv$), respectively. Lee et al. [110] produce ethylidyne fragments on Pt (111) by dissociative adsorption of 1,1,1-trichloroethane, characterized by a single asymmetric peak at 284.0 eV. The broadened C 1s feature at 284.1 eV in our 250 K spectrum (Figure 16a) is consistent with these observations, and is assigned to the ethylidyne fragments expected from the dissociative adsorption of 1,1,1-trichloroethane and consistent with the chemistry observed in TPD attributed to the reaction of ethylidyne fragments.

The high binding energy tail at 288 eV in the 250 K spectrum of Figure 16 is attributed to the presence of molecular CH_3CCl_3, which desorbs at 330 K in TPD (Figure 12). The dominant feature in the 250 K spectrum is at 284.1 eV indicating ethylidyne is bound to surface Cr cations rather than O anions since C 1s binding energies for oxygenated carbons (e.g., alkoxides, carboxylates, and carbonates) typically fall at binding energies of 286 eV or greater [33,55]. We cannot, however, completely rule out the possibility of O-atom-bound ethylidyne since the tail extending to 288 eV in the 250 K is in the binding energy range characteristic of both chlorinated and oxygenated carbon.

Heating to temperatures up to 800 K removes the majority of the surface bound hydrocarbon species, consistent with the evolution of carbon-containing reaction products in this temperature range in TPD. In contrast to post-reaction AES results, a small

amount of surface carbon remains after heating to 800 K. This difference is thought to be due to uptake of residual background gas in the chamber from sequential 44 L exposures of CH_3CCl_3 using the backfill method. A similar amount of surface C is also observed at the same binding energy as that of the 800 K spectrum from a blank after heating to 800 K without any deliberate exposure to CH_3CCl_3.

The Cl 2p spectra shown in Figure 16b exhibit a similar trend to the C 1s data. A higher binding energy Cl 2p feature is observed following the dose, and the higher binding energy feature is lost as a result of heating. The Cl 2p spectrum collected after the dose at 150 K is characteristic of a single unresolved Cl 2p doublet with a Cl $2p_{3/2}$ binding energy of 200.2 eV. Heating to 250 K results in the loss of the high binding energy feature, and leaves a contribution primarily associated with a single unresolved Cl 2p doublet with a Cl $2p_{3/2}$ feature at 198.1 eV. Similar to the assignment for C 1s, the high binding energy features are attributed to Cl in molecular CH_3CCl_3, with the low binding energy features attributed to the Cl adatom surface reaction product. This low binding energy of the remaining Cl 2p doublet (Cl $2p_{3/2}$ at 198.1 eV) is characteristic of metal chloride [33], and is assigned to Cl adatoms bound at surface Cr sites. These XPS observations support earlier reports of the capping of surface Cr cations by halogen adatoms [17-21,62].

4.3 Discussion

4.3.1. Initial dissociation

The thermal decomposition of 1,1,1-trichloroethane on α-Cr_2O_3 ($10\bar{1}2$) primarily results in surface Cl adatoms and surface ethylidyne fragments. The presence of trace amounts of vinyl chloride in TPD suggests that incomplete dissociation can occur

following the initial deposition of Cl adatoms on the surface. As suggested above, it is likely that this incomplete dissociation process occurs on partially chlorinated regions of the surface, with complete dissociation requiring multiple vacant cation sites to accommodate the organic ligand and three Cl atoms. Similar observations of incomplete dissociation were reported for the reaction of 1,1-dichloroethane on the α-Cr_2O_3 ($10\bar{1}2$) surface [18]. In contrast to previous observations of halo-hydrocarbon chemistry on this surface [17-21,53,62], the Cl coverage levels off at ~60% of a monolayer and the chemistry persists at 20% of its initial intensity. This suggests that while the majority of reactive Cr cations sites on the surface are blocked by Cl adatoms, the surface can still facilitate complete dissociation of small amounts of 1,1,1-trichloroethane.

4.3.2. Ethylidyne binding modes

The ethylidyne fragment is thought to bind at a single Cr cation site on the α-Cr_2O_3 ($10\bar{1}2$) surface similar to ethylidyne bound to the single Cr center in the organometallic complex $(CH_3C)Cr(CO)_4Br$ [111]. Justification for this assignment is twofold: nearest-neighbor surface cation sites are ~3.65 Å apart, preventing ethylidyne bridge bonding between cations, and C 1s binding energies in XPS following C-Cl bond cleavage are consistent with a metal-bound intermediate. This atop binding mode is in contrast to four-fold, three-fold or two-fold bridging ethylidyne found in reports for metal surfaces [80,84,90,91,96,103,112,113].

4.3.3. Ethylidyne decomposition

The thermally induced decomposition of ethylidyne on the α-Cr_2O_3 ($10\bar{1}2$) surface leads to gas-phase hydrocarbon products and no surface carbon according to post-reaction AES measurements. The lack of carbon deposition marks a significant

64

difference from work on metal surfaces. To our knowledge, this study describes the first instance of ethylidyne decomposition in UHV (without the presence of excess hydrogen) without carbon deposition. The majority of reports in the literature only describe the decomposition process in terms of the resultant carbon deposition and H_2 desorption [40,44,74,76,83,89,96-101,104,106,107]. The ethylidyne decomposition pathway has been described in more detail in a limited variety of metal surfaces. On Ru(001), ethylidyne decomposition is thought to proceed by β-hydrogen elimination to vinylidene which further decomposes to surface carbon and H_2 desorption [78,79,94]. In one report on Ru(001), a methyne (CH≡) fragment is identified, suggesting that decomposition of vinylidene proceeds by C-C bond scission [94]. Methyne is also observed from ethylidyne decomposition on W(110) and C/W(110), again indicative of C-C bond scission leading to surface carbon deposition [105]. On both Pt(111) [77] and Rh(100) [86], ethylidyne decomposition proceeds by hydrogen elimination to ethynyl (−C≡CH) fragments, followed by C-C bond scission to methyne which decomposes further to yield carbon deposition and H_2 desorption. In all instances where the ethylidyne decomposition pathway is described, C-C bond scission appears to be an important part of the pathway leading to carbon deposition.

In the present case, the ethylidyne reaction proceeds by β-elimination to form vinylidene (4.2), which subsequently isomerizes by a 2,1-hydrogen shift to form acetylene (4.3) [21]. A strong backbonding character of metal centers to the anti-bonding π* orbital of adsorbed vinylidene is known to weaken the C=C bond, leading to an increase in the C=C bond distance and enhancing the possibility of C-C bond scission [114]. The weak backbonding character of surface Cr cations on α-Cr_2O_3 (10$\bar{1}$2) appears

to favor the intramolecular isomerization of vinylidene by a 2,1-hydrogen shift to HC≡CH rather than C-C bond scission and complete dehydrogenation.

4.3.4. Activity of α-Cr₂O₃ (10$\bar{1}$2)

The Cl adatoms deposited on the nearly-stoichiometric α-Cr$_2$O$_3$ (10$\bar{1}$2) surface during the reaction of 1,1,1-trichloroethane have a significant impact on the activity of the surface. The observed binding energy of the Cl adatoms in XPS is consistent with metal chloride, and indicates that Cl adatoms block active Cr^{3+} sites for the reaction, consistent with earlier reports [17,18]. In the catalysis literature, deactivation of powdered Cr$_2$O$_3$ catalysts has been attributed to carbon deposition [57], and to the formation of inactive crystalline phases at the surface that isolate cations from the surface [58]. In this work, no new crystalline phases are observed as a result of reaction; the LEED pattern (not shown) retains the (1x1) periodicity of the nearly-stoichiometric surface. Likewise, no carbon residue is deposited on the α-Cr$_2$O$_3$ (10$\bar{1}$2) surface as a result of the reaction of ethylidyne. These results suggest that under the conditions of this study ethylidyne fragments are not a major intermediate in coke production on (10$\bar{1}$2) facets, where the available cation and anion sites expose primarily a single coordination vacancy.

4.4 Conclusions

The reaction of ethylidyne species was examined on the nearly-stoichiometric α-Cr$_2$O$_3$ (10$\bar{1}$2) surface under UHV conditions via the dissociative adsorption of CH$_3$CCl$_3$. The reaction of ethylidyne fragments primarily yields HC≡CH, CH$_2$=CH$_2$ and H$_2$; however, trace amounts of 2-butyne and CH$_2$=CHCl are also observed. The rate-limiting surface reaction step for the primary chemistry is dehydrogenation of ethylidyne to

vinylidene and hydrogenation of ethylidyne to ethylidene. Vinylidene and ethylidene both react by an intramolecular 2,1-hydrogen shift to form HC≡CH and CH_2=CH_2, respectively. Chlorine adatoms from the decomposition reaction gradually deactivate the surface to C-Cl bond cleavage by simple Cr^{3+} site blocking. No surface carbon is observed in post-reaction AES indicating that ethylidyne species are not primary coke forming intermediates on $(10\bar{1}2)$ facets of α-Cr_2O_3 under the conditions of this study.

Chapter 5

Structure sensitive water interactions with model chromia surfaces: D_2O on α-Cr_2O_3 $(10\bar{1}2)$ and (0001)

5.1 Introduction

Demonstrations of structure-sensitive reactivity on single crystal and thin-film oxide surfaces are facilitated by the ability to control the local coordination environment of surface cations and anions. These surface sites are usefully described by their coordination number and oxidation state, and the chemical nature of the surface can often be linked to these properties. For example, in thermal desorption of acetic acid on the (0001) polar surfaces of ZnO [61], acetic acid desorbs intact from the O-polar surface which exposes O anions with zero coordination vacancies per surface Zn cation. In contrast, the Zn-polar surface which exposes Zn cations with a single coordination vacancy dissociates acetic acid to form stable surface acetate species. In this way, the reactivity of acetic acid on the ZnO surfaces is related to the coordination number of surface Zn cations. This paper demonstrates that a thermal desorption experiment with a water probe molecule on single crystal surfaces of chromium oxide (α-Cr_2O_3) can provide a structure sensitive interaction associated with the Cr cation coordination number.

Since water is a weak Brønsted acid, dissociation can be thought of as a heterolytic process forming H^+ and OH^-. The site-pair requirements for the dissociation reaction on metal-oxide surfaces are best described in terms of Lewis acidity and basicity. The electron deficient cation (Cr^{3+}) sites are Lewis acids and accommodate the hydroxyl

species, while the electron-rich anion (O^{2-}) sites are basic and bind the acid proton to form a second surface hydroxyl [61,115].

In the literature, there are three experimental studies on the interaction of water with thin-film α-Cr_2O_3 (0001) surfaces grown on either Cr(110) [116,117], α-Fe_2O_3 (0001) [31] or α-Al_2O_3 (0001) [31] single crystal surfaces. In the first study, Freund's group reported ARUPS results of water adsorbed on α-Cr_2O_3 (0001)/Cr(110) thin films [116]. They found that molecular water is completely desorbed at 270 K and hydroxyl groups are observed to about 500 K. The low intensity of the hydroxyl feature in ARUPS lead to the conclusion that hydroxyl groups are only formed at surface defect sites. In the second study, Henderson and Chambers reported HREELS, TPD and XPS data for water adsorbed on α-Cr_2O_3 (0001) thin films grown on α-Fe_2O_3 and α-Al_2O_3 [31]. In their report, the assignment of defect sites for hydroxyl formation was not confirmed. Instead, it was concluded that water adsorbs dissociatively on terrace sites following the acid-base site-pair model described above, with a second water molecule binding in molecular form to the same cation surface site. In the most recent study, Maurice et al. reported XPS, TPD, LEED and STM data for the interaction of water with α-Cr_2O_3 (0001)/Cr(110) thin-films [117]. They confirmed the findings of Henderson and Chambers [31] that hydroxylation of the surface occurs via dissociative adsorption at terrace sites as well as defect sites.

In this report, we present TPD results on the interaction of water with the nearly-stoichiometric α-Cr_2O_3 (0001) and ($10\bar{1}2$) single crystal surfaces. We confirm prior reports of multiple water molecules coordinated to a single Cr surface cation on the (0001) surface. By comparing TPD desorption features we conclude that chemisorbed

water dissociates on the $(10\bar{1}2)$ surface, but that only a single water molecule is coordinated to each surface cation. We also present TPD evidence for defect chemistry on an ion-bombarded and annealed (0001) surface which produces hydrogen.

5.2 Results

5.2.1. Nearly-stoichiometric α-Cr$_2$O$_3$ (0001)

The coverage dependence of the D_2O desorption traces from a clean, nearly-stoichiometric α-Cr$_2$O$_3$ (0001) surface following adsorption at 100 K is shown in Figure 17. For clarity the top and bottom portions of the figure display the larger and smaller exposures and TPD traces of D_2O, respectively. All TPD desorption traces and quantities have been corrected for mass spectrometer sensitivity.[12] D_2O is the only desorption product observed in TPD; no D_2 or O_2 are detected. At the lowest exposure investigated, 0.15 L (1L $\equiv 10^{-6}$ Torr-s), a single D_2O peak is observed with a peak maximum at 475 K. For exposures of 0.3 L or greater a second feature is observed at 410 K. While the two features are not well-resolved, it appears that the 475 and 410 K desorption features have peak temperatures that are invariant with increasing coverage indicative of first-order kinetics. For exposures exceeding 0.4 L a broad, low-temperature feature near 250 K appears and grows towards lower temperature with increasing coverage. For a 2 L exposure, a sharp feature is observed at 175 K, increasing to ~180 K for a 3 L exposure with a leading edge overlapping for 3, 2.5 and 2 L exposures. This behavior is characteristic of zeroth-order desorption kinetics associated with multilayer formation. Multilayer water desorption is typically reported at ~160 K.

---

[12] Relative mass spectrometer sensitivity factors of 0.28 for D_2O (m/z 20) and 2.64 for D_2 (m/z 4) were determined experimentally.

Figure 17. TPD traces ranging from 0.15 to 3 L adsorption on a nearly-stoichiometric α-Cr_2O_3 (0001) surface show D_2O (m/z 20) desorption trends. The upper plot shows larger doses and the lower plot displays smaller doses scaled to magnify the chemisorbed water features above 250 K. The baselines have been offset for clarity.

5.2.2. Ion bombarded and annealed α-Cr$_2$O$_3$ (0001)

TPD from a series of 1 L D$_2$O exposures and TPD runs on the ion bombarded and annealed α-Cr$_2$O$_3$ (0001) surface yields a D$_2$ (m/z 4) desorption feature at ~810 K shown in Figure 18. The D$_2$ feature shrinks in size with each successive dose through the series of exposures. The peak temperature is independent of amount indicative of first-order desorption kinetics. The D$_2$O (m/z 20) TPD features from the ion bombarded and annealed (0001) surface (not shown) are identical to those observed from the nearly-stoichiometric surface. D$_2$O and D$_2$ are the only desorption products observed from the ion bombarded and annealed (0001) surface; no O$_2$ is detected. The inset of Figure 18 shows the integrated peak intensities of the D$_2$ and D$_2$O features from the same experiment (note the scale factor of 10^3 for D$_2$). The selectivity to D$_2$ from the chemisorbed layer (>250 K) of the first 1 L D$_2$O exposure and TPD run is less than 1 %.

5.2.3. Nearly-stoichiometric α-Cr$_2$O$_3$ (10$\bar{1}$2)

The coverage dependence of the D$_2$O desorption traces from a clean, nearly-stoichiometric α-Cr$_2$O$_3$ (10$\bar{1}$2) surface following adsorption at 100 K is shown in Figure 19. D$_2$O is the only desorption product observed in TPD; no D$_2$ or O$_2$ are detected. At the lowest exposure investigated, 0.05 L, a single D$_2$O peak is observed with a peak maximum at 470 K. The peak temperature increases to ~480 K with increasing coverage suggestive of pseudo zeroth-order kinetics [118]. Similar to the (0001) surface, for exposures exceeding 0.4 L a broad feature grows towards lower temperatures, and a sharp feature is observed beginning at ~170 K for a 0.8 L exposure, increasing to 170 K for a 3 L exposure. The sharp feature with overlapping leading edges is indicative of zeroth order desorption kinetics, attributed to multilayer D$_2$O desorption.
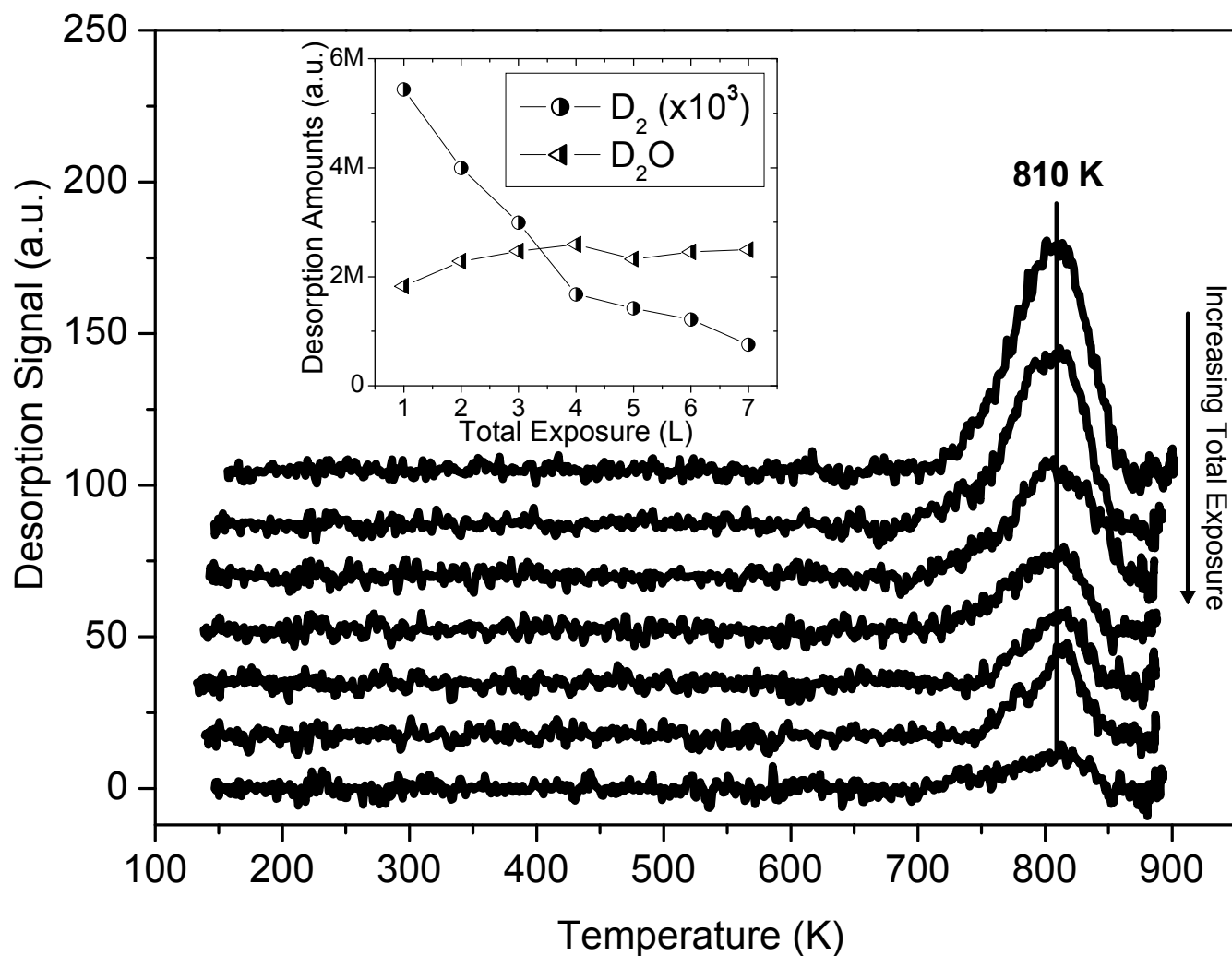
Figure 18. TPD traces following D_2 (m/z 4) production from a series of 1 L D_2O exposures on the ion bombarded and annealed α-Cr_2O_3 (0001) surface. The inset of the figure shows integrated TPD peak areas of the D_2 and D_2O desorption features (note the scale factor applied to the D_2 signal). The baselines have been offset for clarity.
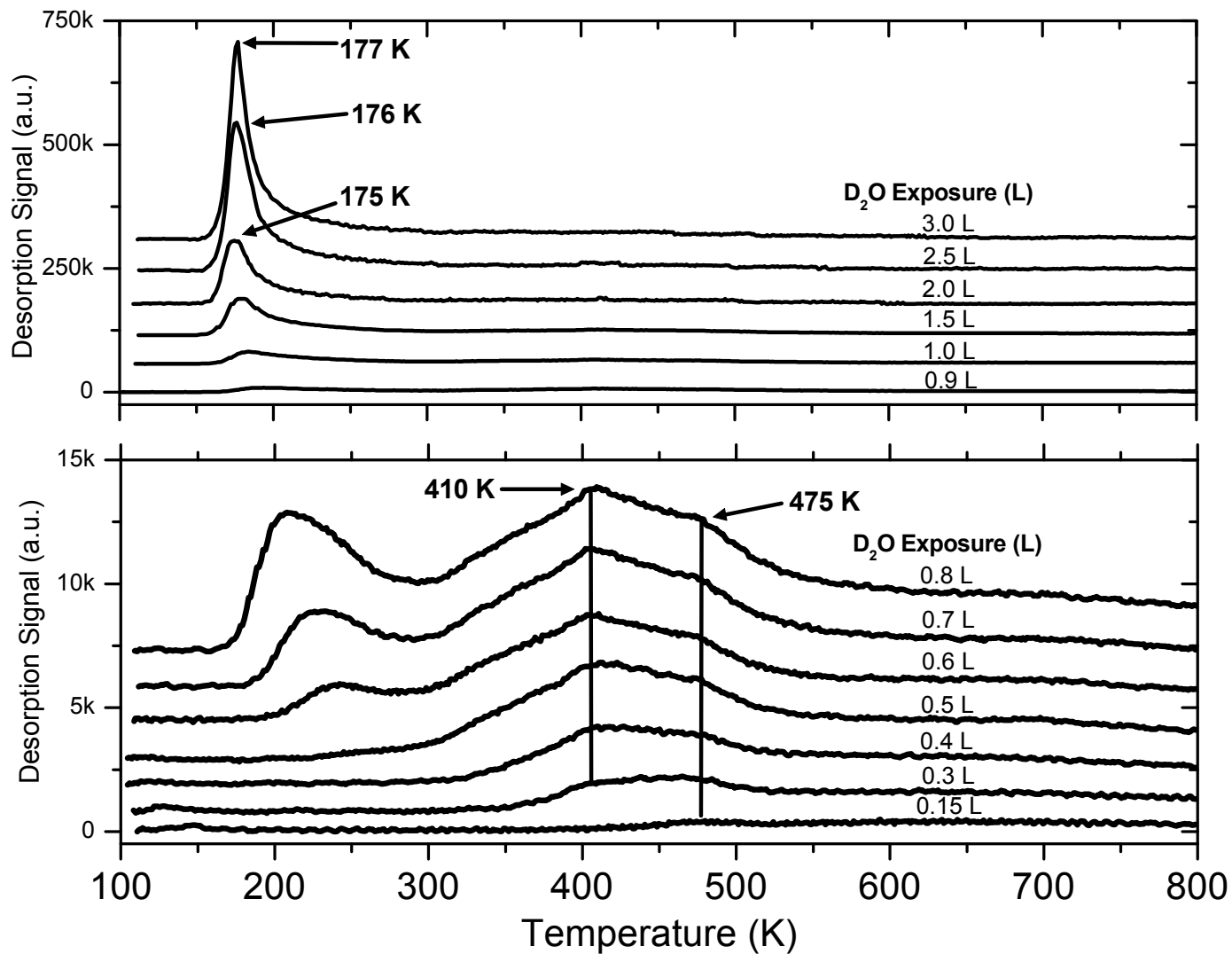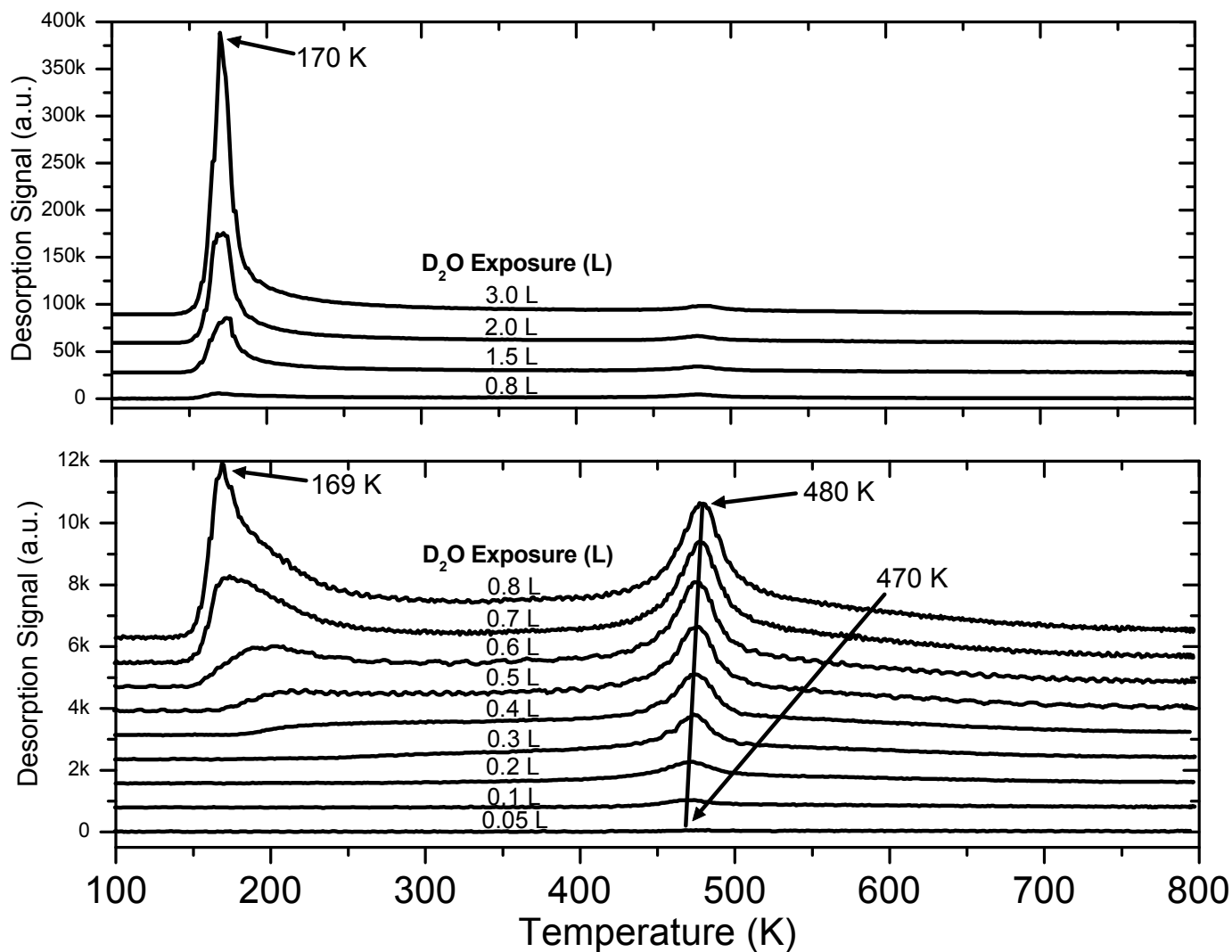
Figure 19. TPD traces ranging from 0.05 to 3 L adsorption on a nearly-stoichiometric α-Cr_2O_3 $(10\bar{1}2)$ surface show D_2O (m/z 20) desorption trends. The upper plot shows larger doses and the lower plot displays smaller doses scaled to magnify the chemisorbed water feature above 400 K. The baselines have been offset for clarity.

5.3 Discussion

5.3.1. D$_2$O TPD on nearly-stoichiometric α-Cr$_2$O$_3$ (0001)

The previous two TPD studies of water on thin-film α-Cr$_2$O$_3$ (0001) surfaces report a variety of desorption temperatures for chemisorbed water features (above 250 K). In the first report, Henderson and Chambers report two desorption features at 295 and 345 K, and attribute them to molecular and dissociatively adsorbed water, respectively [31]. In a following report, Maurice et al. report a broad feature with two poorly resolved peaks in the range of 400-420 K and 470-500 K [117], higher by ~100 K than the features in the report of Henderson and Chambers. Maurice et al. attribute the broad desorption profile to the recombination of surface hydroxyl species. Unlike the assignment of Henderson and Chambers, the poorly resolved, low temperature feature is not attributed to molecular water, based on citations that molecular water is not observed above 300 K in ultrahigh vacuum [22,119].

In Figure 17, we report two poorly resolved D$_2$O desorption features in TPD at 410 and 475 K. The temperatures of these two features are similar to the temperatures reported in TPD by Maurice et al. [117], but are much higher in temperature than those reported by Henderson and Chambers [31]. We attribute the temperature differences to the experimental differences in thermocouple attachment procedures. Henderson and Chambers cement their thermocouple into a horizontal edge slot of the substrate crystal, and Maurice et al. press their thermocouple to the sample surface during the heating ramp for TPD [117]. In our work, the thermocouple is cemented to the back of the single crystal through a hole in the tantalum stage. The method employed by Henderson and Chambers is likely the most accurate for two reasons: the thermocouple is embedded in

the substrate, excluding the possibility of sampling the temperature from the mounting hardware used for resistive heating of the crystal, and the thermocouple is cemented in place, ensuring that good thermal contact is maintained with the crystal substrate. The method employed by Maurice et al. likely yields higher desorption temperatures because the thermocouple is not cemented in place, preventing sufficient thermal contact with the sample surface. The method employed in our study likely yields higher readings because the temperature is measured at the back of the sample adjacent to the resistively heated Ta sample mount. Therefore, by analogy to the study of Henderson and Chambers [31], we assign the D_2O desorption feature at 475 K to the recombination of dissociated water, and the 410 K feature to desorption of a molecular D_2O surface species.

The first-order desorption kinetics of the D_2O feature at 475 K in TPD on the nearly-stoichiometric (0001) surface is counterintuitive since the elementary recombination process is second-order. Similar observations of a lack of correspondence between the kinetics and the elementary reaction process have been reported for other systems. For water TPD on thin-film α-Cr_2O_3 (0001), Henderson and Chambers suggest that the recombination peak for water at 345 K is first-order in acid-base site pairs required for dissociation [31]. In a report of water TPD on Cu_2O (001), Schulz and Cox suggest that the rate-limiting step for water recombination is Cu^+-O bond breaking to produce a freely diffusing hydroxyl adduct for subsequent recombination [120]. While these explanations are speculative, they may apply to the first-order recombination peak in TPD at 475 K in this report.

5.3.2. D$_2$O TPD on nearly-stoichiometric α-Cr$_2$O$_3$ (10$\bar{1}$2)

The D$_2$O feature at ~480 K in TPD on the α-Cr$_2$O$_3$ (10$\bar{1}$2) surface can be

attributed to recombination of dissociated water based on the high temperature of the

peak [22,119] and the comparable temperature to the recombination reaction on the

nearly-stoichiometric (0001) surface. In contrast to the two TPD features observed at 475

and 410 K on the nearly-stoichiometric (0001) surface, only a single feature is observed

at ~480 K on the nearly-stoichiometric (10$\bar{1}$2) surface. This difference is ascribed to the

difference in coordination number of Cr cations exposed on the two surfaces. The

nearly-stoichiometric (10$\bar{1}$2) surface exposes Cr cations with only a single coordination

vacancy, while the nearly-stoichiometric (0001) surface exposes Cr cations with three

coordination vacancies, allowing for multiple D$_2$O molecules to interact with the same

surface Cr cation.

The recombination peak for D$_2$O in TPD exhibits pseudo-zeroth order kinetics.

Again, this behavior is counterintuitive since the expected elementary reaction process

for recombination of surface hydroxyl species is second-order. This behavior is not

understood, but is also not unprecedented in the surface science literature. On the

reconstructed, (2 x 1) surface of the α-Fe$_2$O$_3$ (10$\bar{1}$2) surface, the water recombination

feature in TPD exhibits pseudo zeroth-order kinetics [118]. It has been suggested that

recombination of surface hydroxyl species occurs at the ends of 1-dimensional islands of

hydroxyl species running along the corrugated rows of the surface. The (2 x 1)

reconstruction of the α-Fe$_2$O$_3$ (10$\bar{1}$2) surface is produced by annealing the (1 x 1) surface

to 900 K in UHV, inducing reduction of the surface and doubling of the periodicity in the

[10$\bar{1}$0] direction. According to LEED and EELS data reported, every other row retains

(1 x 1)-like structure and the recombination peak is attributed to OH bound to the unmodified, (1 x 1)-like rows. In effect, the reconstructed surface enhances island formation by segregating the surface into a patchwork of (2 x 1) and (1 x 1) structures. While the $(10\bar{1}2)$ surface in this study is not reconstructed and exhibits only a (1 x 1) structure, a similar phenomenon may be responsible for the pseudo zeroth-order kinetics observed on this surface as well given the channels running along the $[02\bar{2}1]$ direction (Figure 1).

5.3.3. D_2O TPD on ion-bombarded and annealed α-Cr_2O_3 (0001)

The interaction of D_2O with the ion-bombarded and annealed (0001) surface produces a D_2 feature in TPD that is not observed from the nearly-stoichiometric (0001) surface. The gradual decline of the D_2 peak by successive 1 L D_2O exposures and TPD runs indicates that the reaction leading to water reduction and D_2 production also consumes the active site for D_2 production. This behavior, along with the lack of O_2 desorption in TPD, is consistent with the irreversible consumption of O atoms at a small minority of oxygen-deficient, reduced Cr surface sites. Similar observations of irreversible dissociation of water on reduced CeO_2 and Rh/CeO_2 surfaces was assigned to the oxidation of O-deficient Ce^{3+} cations leading to H_2 production above 500 K [121]. The kinetics of the D_2 production in TPD (Figure 4) are first-order, indicating that the rate-limiting step for desorption is not simply the recombination of two deuterium atoms, a second-order process. The first-order kinetics suggests that the rate-limiting step may be associated with either the migration of deuterium atoms bound at surface lattice oxygen sites, or the decomposition of a hydroxyl group bound at a reduced Cr surface site, leaving behind an irreversibly bound O atom. Since the recombination of hydrogen

78

atoms to H_2 occurs at 285 K [21], the possibility associated with deuterium migration can be ruled out. Therefore, the first-order kinetics are likely associated with the decomposition of a hydroxyl group bound at a reduced Cr surface cation site. The population of reduced sites associated with the D_2 formation in TPD on the ion bombarded and annealed (0001) surface is less than 1 % of the total surface Cr site density.[13]

5.4 Conclusions

The interaction of D_2O with the surfaces of α-Cr_2O_3 is structure sensitive. We have demonstrated the sensitivity of water to the coordination number of Cr^{3+} surface cations. In TPD, two D_2O features are observed for chemisorbed water (>250 K) from the nearly-stoichiometric (0001) surface which exposes three coordination vacancies, while a single chemisorbed D_2O feature is observed from the nearly-stoichiometric $(10\bar{1}2)$ surface which exposes Cr cations with a single coordination vacancy. We have also observed that reduced Cr surface sites irreversibly bind O atoms from dissociatively adsorbed D_2O to produce D_2 in TPD.

---

[13] Estimates of defect site populations were calculated assuming: (1) unity sticking coefficient for D_2O exposures at 100 K; (2) defect site ratio based on the relative amounts of D_2 and D_2O in the chemisorbed layer (>250 K in TPD); (3) total Cr surface site density on the (0001) surface of 4.69 x 10^{14} Cr/cm^2.

Chapter 6

Summary and Recommendations for Future Work

6.1 Summary

6.1.1. Selectivity of C$_2$-alkyl fragment reactions on nearly-stoichiometric α-Cr$_2$O$_3$ (10$\bar{1}$2)

In terms of ethane dehydrogenation to ethylene, the selectivity is dependent on the

C$_2$-alkyl fragment formed from ethane on (10$\bar{1}$2) facets of α-Cr$_2$O$_3$. Both ethyl and

ethylidene intermediates are selective towards ethylene. However, ethylidyne is more

selective towards acetylene, but also produces ethylene as a secondary reaction product.

The pathways to the production of ethylene are dependent on the C$_2$-alkyl fragment.

Ethylene is produced from ethyl fragments by β-elimination, from ethylidene by an

intramolecular isomerization and from ethylidyne by self hydrogenation to ethylidene and

subsequent intramolecular isomerization.

In the catalysis literature, deactivation of Cr$_2$O$_3$ dehydrogenation catalysts has

been attributed to carbon deposition [57], and to the formation of inactive crystalline

phases at the surface that isolate cations from the surface [58]. In this work, no carbon

deposition has been observed from C$_2$-alkyl fragment reactions over the nearly-

stoichiometric α-Cr$_2$O$_3$ (10$\bar{1}$2) surface. The dichotomy between the dominance of

carbon deposition in the catalysis literature and the complete lack of it in this UHV

surface science study is a surprising result considering that the most likely exposed face

on microcrystalline powders of α-Cr$_2$O$_3$ is (10$\bar{1}$2) [26]. Two possible explanations may

be related to the production of C$_2$-alkyl fragments in this study by dissociative adsorption

of chlorinated ethanes. For one, the Cl adatoms from dissociation block further

interaction with active Cr surface cations, preventing multiple turnovers on the same site. Therefore, if carbon deposition is a low probability reaction channel on the surface in comparison to other reaction pathways, the likelihood of observing it from a single turnover per site is small. Secondly, production of C_2-alkyl fragments by C-Cl bond cleavage circumvents the activation barriers necessary for C-H bond cleavage directly from ethane, which have been shown to thermodynamically favor cracking reactions leading to lighter alkanes and carbon deposition [2]. A third possibility, considered the most likely explanation based on the experimental evidence, may be that the active site for C-C bond cleavage on powdered Cr_2O_3 dehydrogenation catalysts is not displayed on the nearly-stoichiometric α-Cr_2O_3 ($10\bar{1}2$) surface.

Ethylidene coupling to 2-butene and ethylidyne coupling to 2-butyne are an indication of the mobility of pi-bonded systems on the nearly-stoichiometric α-Cr_2O_3 ($10\bar{1}2$) surface. This phenomena has also been reported for methylene [19,62] and vinyl fragments [18] on the ($10\bar{1}2$) surface. While ethylidene, ethylidyne, methylene and vinyl fragments migrate to form coupling products, no migration is observed for ethyl, methyl [19] or vinylidene [21] fragments, suggesting that either a lack of pi-bonded systems near the surface (ethyl and methyl) or two pi-bonded systems near the surface (vinylidene) results in a lower activation barrier to other reaction processes (i.e. β-elimination, α-elimination or isomerization). It is not understood how the size of the hydrocarbon fragment and/or the position of pi-bonds with respect to the surface affects the activation barrier to migration. Furthermore, the activation barrier to migration of ethylidene and ethylidyne is unknown since both 2-butene and 2-butyne coupling products exhibit

desorption limited kinetics in TPD. Therefore, a direct comparison between ethylidene, ethylidyne, vinyl and methylene migration processes cannot be made.

6.1.2. Structure sensitive water interactions with α-Cr$_2$O$_3$ (0001) and (10$\bar{1}$2) surfaces

The interaction of water with the nearly-stoichiometric α-Cr$_2$O$_3$ (0001) and (10$\bar{1}$2) surfaces is *structure sensitive*. Water is sensitive to the difference in coordination number of Cr surface cations between the two surfaces, and on the α-Cr$_2$O$_3$ (0001) surface, water has also demonstrated sensitivity to the degree of surface Cr cation reduction (and/or reduced coordination). These observations allowed for the development of a surface treatment recipe for the nearly-stoichiometric (0001) surface. The recipe was derived by quantification of surface Cr cation reduction in tandem with modification of the surface preparation method. The ability to prepare the nearly-stoichiometric α-Cr$_2$O$_3$ (0001) surface opens the door to future studies.

6.2 Suggested Future Work

6.2.1. Structure sensitivity of C$_2$-alkyl fragment reactions

Preliminary studies of C$_2$-alkyl fragment chemistry on the α-Cr$_2$O$_3$ (0001) surface exhibited clear signs of *structure sensitivity* due to the reduced coordination of surface Cr cations relative to the cations on the (10$\bar{1}$2) surface. Therefore, continued work with small hydrocarbon fragments on the nearly-stoichiometric α-Cr$_2$O$_3$ (0001) surface is certainly warranted. Future work should focus on understanding the changes in the (0001) surface due to halogen deposition from dissociative adsorption of chlorinated hydrocarbon compounds. This may be accomplished by examining the interaction of probe molecules in TPD in tandem with the deposition of halogen from halo-hydrocarbon

reactions. Therefore, it may be possible to relate the changes in the chemistry due to halogen deposition to the specific surface ensembles responsible.

6.2.2. Transition state of β-elimination from ethyl reactions on α-Cr$_2$O$_3$ (10$\bar{1}$2)

The reaction of ethyl fragments on the nearly-stoichiometric α-Cr$_2$O$_3$ (10$\bar{1}$2) surface proceeds by β-elimination forming ethylene product and liberating hydrogen atoms to the surface. The transition state of the elimination reaction is termed β-hydride elimination based on ample precedence in the surface science literature for ethyl reactions on metal surfaces [15,35,36,38-47,49]. However common β-hydride elimination may be for hydrocarbon fragments with carbons in the beta position, no direct experimental evidence is presented in this study to conclusively demonstrate whether the reaction should be termed a proton, hydrogen or hydride elimination. This lack of direct evidence provides an interesting experimental opportunity. Experimental determination of the transition state is typically achieved by utilization of substituent inductive effects. For instance, the activation barrier to propyl fragment β-elimination reactions on Pt (111) increases as the hydrogens on the methyl end of the molecule are sequentially substituted for fluorine atoms [122]. The electronegativity of the fluorine substituents withdraws electron density via an inductive effect which can stabilize the transition state, destabilize the transition state or cause no change at all. In this way, the charge distribution in the transition state can be deduced simply based on the experimental desorption kinetics. I propose that a series of fluorinated ethyl fragments (i.e. chloroethane, 1-chloro-2-fluoroethane, and 1-chloro-2,2-difluoroethane) be studied on the nearly-stoichiometric α-Cr$_2$O$_3$ (10$\bar{1}$2) surface in an effort to elucidate the nature of the transition state for β-elimination reactions.

6.2.3. Coke formation from ethane, ethylene and acetylene by C-C bond scission

The questions that arise about the lack of carbon deposition under the conditions of this study provide an interesting experimental opportunity. In TPD, ethane, ethylene and acetylene adsorbed at 100 K desorbs intact at 170, 290 and 310 K, respectively, and no carbon deposition is observed [51]. It may be possible to deposit carbon from ethane, ethylene or acetylene on the nearly-stoichiometric α-Cr_2O_3 ($10\bar{1}2$) surface by exposing the surface to the respective molecules at elevated temperatures. Following the amount of carbon in post-reaction AES, if carbon deposition occurs, one would expect a step-change at some threshold hydrocarbon molecule exposure temperature. The conditions of this experiment would likely mimic the steady state conditions of ethane dehydrogenation over powdered Cr_2O_3 catalyst and may provide a more realistic measure of the probability for carbon deposition on ($10\bar{1}2$) facets of α-Cr_2O_3. Additionally, it may be possible to monitor steady-state product production during the exposure using the same mass spectrometer techniques employed during TPD for gas phase product identification.

References

[1]   J.E. Germain, Catalytic Conversion of Hydrocarbons, New York, NY, Academic Press, Inc., 1969.

[2]   B.M. Weckhuysen, R.A. Schoonheydt, Catalysis Today 51 (1999) 223.

[3]   U. Olsbye, A. Virnovskaia, O. Prytz, S.J. Tinnemans, B.M. Weckhuysen, Catalysis Letters 103 (2005) 143.

[4]   D.W. Flick, M.C. Huff, Applied Catalysis a-General 187 (1999) 13.

[5]   B. Grzybowska, J. Sloczynski, R. Grabowski, L. Keromnes, K. Wcislo, T. Bobinska, Applied Catalysis a-General 209 (2001) 279.

[6]   S. Wang, K. Murata, T. Hayakawa, S. Hamakawa, K. Suzuki, Chemistry Letters (1999) 25.

[7]   S.B. Wang, K. Murata, T. Hayakawa, S. Hamakawa, K. Suzuki, Chemistry Letters (1999) 569.

[8]   S.B. Wang, K. Murata, T. Hayakawa, S. Hamakawa, K. Suzuki, Applied Catalysis a-General 196 (2000) 1.

[9]   Y.R. Luo, J.L. Holmes, Journal of Physical Chemistry 98 (1994) 10368.

[10]   Y.R. Luo, J.L. Holmes, Journal of Physical Chemistry 98 (1994) 303.

[11]   M.X. Yang, S. Sarkar, B.E. Bent, S.R. Bare, M.T. Holbrook, Langmuir 13 (1997) 229.

[12]   C.W. Chan, A.J. Gellman, Catalysis Letters 53 (1998) 139.

[13]   T.V.W. Janssens, F. Zaera, Journal of Physical Chemistry 100 (1996) 14118.

[14]   G. Wu, D. Stacchiola, M. Kaltchev, W.T. Tysoe, Journal of the American Chemical Society 122 (2000) 8232.

[15]   M.X. Yang, S.K. Jo, A. Paul, L. Avila, B.E. Bent, K. Nishikida, Surface Science 325 (1995) 102.

[16]   G. Zhou, C. Chan, A.J. Gellman, Journal of Physical Chemistry B 103 (1999) 1134.

[17]   J.D. Brooks, Q. Ma, D.F. Cox, Surface Science 603 (2009) 523.

[18]   M.A. McKee, Q. Ma, D.R. Mullins, M. Neurock, D.F. Cox, Surface Science 603 (2009) 265.

[19]   C.M. Byrd, Reaction Chemistry of C_1 Hydrocarbon Fragments and Oxygenates on Cr_2O_3 (1012), Blacksburg, VA 24060, Virginia Polytechnic Institute and State University, 2003.

[20]   S.C. York, D.F. Cox, Journal of Physical Chemistry B 107 (2003) 5182.

[21]   S.C. York, D.F. Cox, Journal of Catalysis 214 (2003) 273.

[22]   M.A. Henderson, Surface Science Reports 46 (2002) 5.

[23]   D. Adler, Solid State Physics 21 (1968) 83.

[24]   V.E. Henrich, Reports on Progress in Physics 48 (1985) 1481.

[25]   P.J. Lawrence, S.C. Parker, P.W. Tasker, Journal of the American Ceramic Society 71 (1988) C389.

[26]   D. Scarano, G. Spoto, S. Bordiga, G. Ricchiardi, A. Zecchina, Journal of Electron Spectroscopy and Related Phenomena 64 (1993) 307.

[27]   S.C. York, M.W. Abee, D.F. Cox, Surface Science 437 (1999) 386.

[28]   R.J. Lad, V.E. Henrich, Surface Science 193 (1988) 81.

[29]   M.W. Mensch, C.M. Byrd, D.F. Cox, Catalysis Today 85 (2003) 279.

[30]   F. Rohr, M. Baumer, H.J. Freund, J.A. Mejias, V. Staemmler, S. Muller, L. Hammer, K. Heinz, Surface Science 372 (1997) L291.

[31]   M.A. Henderson, S.A. Chambers, Surface Science 449 (2000) 135.

[32]   L.E. Davis, N.C. MacDonald, P.W. Palmberg, G.E. Riach, R.E. Weber, Handbook of Auger Electron Spectroscopy, Eden Prairie, Minnesota, Physical Electronics Industries, Inc., 1976.

[33]   J.F. Moulder, W.F. Stickle, P.E. Sobol, K.D. Bomben, Handbook of X-ray Photoelectron Spectroscopy, Eden Prairie, Minnesota, Perkin-Elmer Corporation, Physical Electronics Division, 1992.

[34]   Quadrex 200 Residual Gas Analyzer Manual, NY, Leybold Inficon Inc., 1989.

[35]   B.E. Bent, R.G. Nuzzo, B.R. Zegarski, L.H. Dubois, Journal of the American Chemical Society 113 (1991) 1137.

[36]   M.L. Burke, R.J. Madix, Journal of the American Chemical Society 113 (1991) 3675.

[37]   P.A. Coon, M.L. Wise, Z.H. Walker, S.M. George, Surface Science 291 (1993) 337.

[38]   C.J. Jenks, B.E. Bent, F. Zaera, Journal of Physical Chemistry B 104 (2000) 3017.

[39]   L.A. Keeling, L. Chen, C.M. Greenlief, A. Mahajan, D. Bonser, Chemical Physics Letters 217 (1994) 136.

[40]   A. Kis, J. Kiss, D. Olasz, F. Solymosi, Journal of Physical Chemistry B 106 (2002) 5221.

[41]   I. Kovacs, F. Solymosi, Journal of Physical Chemistry 97 (1993) 11056.

[42]   K.G. Lloyd, B. Roop, A. Campion, J.M. White, Surface Science 214 (1989) 227.

[43]   A. Paul, M.X. Yang, B.E. Bent, Surface Science 297 (1993) 327.

[44]   N.K. Singh, A. Bolzan, J.S. Foord, H. Wright, Surface Science 409 (1998) 272.

[45]   F. Solymosi, L. Bugyi, A. Oszko, Langmuir 12 (1996) 4145.

[46]   F. Solymosi, L. Bugyi, A. Oszko, I. Horvath, Journal of Catalysis 185 (1999) 160.

[47]   S. Tjandra, F. Zaera, Surface Science 289 (1993) 255.

[48]   F. Zaera, Journal of the American Chemical Society 111 (1989) 8744.

[49]   H.B. Zhao, B.E. Koel, Catalysis Letters 99 (2005) 27.

[50]   X.L. Zhou, J.M. White, Surface Science 241 (1991) 244.

[51]   J.D. Brooks, D.F. Cox, Unpublished work, 2006.

[52]   P.A. Redhead, Vacuum 12 (1962) 203.

[53]   S.C. York, Halocarbon Reactions on the Cr_2O_3 (1012) Surface, Blacksburg, VA, Virginia Polytechnic Institute and State University, 1999.

[54]   S.K. Jo, J.M. White, Surface Science 245 (1991) 305.

[55]   J.M. Vohs, M.A. Barteau, Surface Science 176 (1986) 91.

[56]   J.L. Lin, B.E. Bent, Journal of Physical Chemistry 96 (1992) 8529.

[57]   L.E. Manzer, V.N.M. Rao, Advances in Catalysis, Vol 39 39 (1993) 329.

[58]   E. Kemnitz, A. Kohne, I. Grohmann, A. Lippitz, W.E.S. Unger, Journal of Catalysis 159 (1996) 270.

[59]   V. Pallassana, M. Neurock, V.S. Lusvardi, J.J. Lerou, D.D. Kragten, R.A. van Santen, Journal of Physical Chemistry B 106 (2002) 1656.

[60]   S. Azad, M. Kaltchev, D. Stacchiola, G. Wu, W.T. Tysoe, Journal of Physical Chemistry B 104 (2000) 3107.

[61]   M.A. Barteau, Journal of Vacuum Science & Technology a-Vacuum Surfaces and Films 11 (1993) 2162.

[62]   C.M. Byrd, M.A. McKee, J.D. Brooks, Y. Dong, D.F. Cox, (2010).

[63]   J.A. Altmann, I.G. Csizmadia, K. Yates, Journal of the American Chemical Society 96 (1974) 4196.

[64]   J.L. Lin, B.E. Bent, Journal of the American Chemical Society 115 (1993) 2849.

[65]   J.L. Lin, B.E. Bent, Journal of Physical Chemistry 97 (1993) 9713.

[66]   F. Zaera, S. Tjandra, Journal of Physical Chemistry 98 (1994) 3044.

[67]   X.L. Zhou, S.R. Coon, J.M. White, Journal of Chemical Physics 94 (1991) 1613.

[68]   J.G. Serafin, C.M. Friend, Journal of the American Chemical Society 111 (1989) 8967.

[69]   K. Domen, T.J. Chuang, Journal of the American Chemical Society 109 (1987) 5288.

[70]   M. Kantcheva, I.G. Dallalana, J.A. Szymura, Journal of Catalysis 154 (1995) 329.

[71]   M. Brookhart, J.R. Tucker, G.R. Husk, Journal of the American Chemical Society 105 (1983) 258.

[72]   G. Dazinger, K. Kirchner, Organometallics 23 (2004) 6281.

[73]   J.N. Andersen, A. Beutler, S.L. Sorensen, R. Nyholm, B. Setlik, D. Heskett, Chemical Physics Letters 269 (1997) 371.

[74]   L. Burkholder, W.T. Tysoe, Journal of Physical Chemistry C 113 (2009) 15298.

[75]   F. Calaza, D. Stacchiola, M. Neurock, W.T. Tysoe, Surface Science 598 (2005) 263.

[76]   D.V. Chakarov, T. Marinova, Surface Science 227 (1990) 310.

[77]   R.P. Deng, E. Herceg, M. Trenary, Surface Science 573 (2004) 310.

[78]   M.M. Hills, J.E. Parmeter, W.H. Weinberg, Journal of the American Chemical Society 109 (1987) 597.

[79]   M.M. Hills, J.E. Parmeter, W.H. Weinberg, Journal of the American Chemical Society 109 (1987) 4224.

[80]   B.E. Koel, B.E. Bent, G.A. Somorjai, Surface Science 146 (1984) 211.

[81]   A.F. Lee, K. Wilson, Journal of Physical Chemistry B 110 (2006) 907.

[82]   D.Y. Lu, C.M. Chiang, Y.W. Yang, X.N. Li, Surface Science 601 (2007) 292.

[83]   T.S. Marinova, D.V. Chakarov, Surface Science 192 (1987) 275.

[84]   T.S. Marinova, K.L. Kostov, Surface Science 181 (1987) 573.

[85]   H.E. Newell, M.R.S. McCoustra, M.A. Chesters, C. De La Cruz, Journal of the Chemical Society-Faraday Transactions 94 (1998) 3695.

[86]   D.L.S. Nieskens, A.P. van Bavel, D.C. Ferre, J.W. Niemantsverdriet, Journal of Physical Chemistry B 108 (2004) 14541.

[87]   B. Schiott, R. Hoffmann, M.K. Awad, A.B. Anderson, Langmuir 6 (1990) 806.

[88]   N.K. Singh, A. Bolzan, Surface Science 358 (1996) 656.

[89]   A.J. Slavin, B.E. Bent, C.T. Kao, G.A. Somorjai, Surface Science 206 (1988) 124.

[90]   A.J. Slavin, B.E. Bent, C.T. Kao, G.A. Somorjai, Surface Science 202 (1988) 388.

[91]   D. Stacchiola, M. Kaltchev, G. Wu, W.T. Tysoe, Surface Science 470 (2000) L32.

[92]   A. Wieckowski, S.D. Rosasco, G.N. Salaita, A. Hubbard, B.E. Bent, F. Zaera, D. Godbey, G.A. Somorjai, Journal of the American Chemical Society 107 (1985) 5910.

[93]   K. Wu, X.M. Wei, Y.M. Cao, D.Z. Wang, X.X. Guo, Catalysis Letters 26 (1994) 109.

[94]   M.C. Wu, D.W. Goodman, Journal of the American Chemical Society 116 (1994) 1364.

[95]   F. Zaera, C.R. French, Journal of the American Chemical Society 121 (1999) 2236.

[96]   T.P. Beebe, J.T. Yates, Surface Science 173 (1986) L606.

[97]   A.F. Carlsson, M. Naschitzki, M. Baumer, H.J. Freund, Surface Science 545 (2003) 143.

[98]   P.A. Dilara, W.T. Petrie, J.M. Vohs, Applied Surface Science 115 (1997) 243.

[99]   M. Frank, M. Baumer, R. Kuhnemuth, N.J. Freund, Journal of Vacuum Science & Technology a-Vacuum Surfaces and Films 19 (2001) 1497.

[100]   D.R. Mullins, Surface Science 556 (2004) 159.

[101]   D.R. Mullins, Surface Science 600 (2006) 2718.

[102]   L. Ovari, F. Solymosi, Langmuir 18 (2002) 8829.

[103]   D.V. Chakarov, T. Marinova, Surface Science 227 (1990) 297.

[104]   B. Fruhberger, J.G. Chen, Journal of the American Chemical Society 118 (1996) 11599.

[105]   H.H. Hwu, J.G.G. Chen, Journal of Physical Chemistry B 107 (2003) 11467.

[106]   H.H. Hwu, J.G.G. Chen, Surface Science 557 (2004) 144.

[107]   B. Vermang, M. Juel, S. Raaen, Journal of Vacuum Science & Technology A 25 (2007) 1512.

[108]   F. Zaera, G.A. Somorjai, Journal of the American Chemical Society 106 (1984) 2288.

[109]   H.P. Bonzel, H.J. Krebs, Surface Science 91 (1980) 499.

[110]   A.F. Lee, P. Carr, K. Wilson, Journal of Physical Chemistry B 108 (2004) 14811.

[111]   G.P. Fouletfonseca, M. Jouan, N.Q. Dao, N.T. Huy, E.O. Fischer, Journal De Chimie Physique Et De Physico-Chimie Biologique 87 (1990) 13.

[112]   R.J. Koestner, M.A. Vanhove, G.A. Somorjai, Surface Science 121 (1982) 321.

[113]   P. Skinner, M.W. Howard, I.A. Oxton, S.F.A. Kettle, D.B. Powell, N. Sheppard, Journal of the Chemical Society-Faraday Transactions Ii 77 (1981) 1203.

[114]   M.R. Albert, J.T. Yates, The Surface Scientists's Guide to Organometallic Chemistry, Washington, DC, American Chemical Society, 1987.

[115]   P.C. Stair, Journal of the American Chemical Society 104 (1982) 4044.

[116]   D. Cappus, C. Xu, D. Ehrlich, B. Dillmann, C.A. Ventrice, K. Alshamery, H. Kuhlenbeck, H.J. Freund, Chemical Physics 177 (1993) 533.

[117]   V. Maurice, S. Cadot, P. Marcus, Surface Science 471 (2001) 43.

[118]   M.A. Henderson, S.A. Joyce, J.R. Rustad, Surface Science 417 (1998) 66.

[119]   P.A. Thiel, T.E. Madey, Surface Science Reports 7 (1987) 211.

[120]   D.F. Cox, K.H. Schulz, Surface Science 256 (1991) 67.

[121]   L. Kundakovic, D.R. Mullins, S.H. Overbury, Surface Science 457 (2000) 51.

[122]   P.P. Ye, A.J. Gellman, Journal of Physical Chemistry B 110 (2006) 9660.